Synthesis of a core-shell silica nanoplatform for multi-modality imaging

Alexander J. Veach[1], Jennifer E. Drewes[2], Brian M. Zeglis[3], Michelle Bradbury[1], Ulrich Wiesner[2], Jason S. Lewis[1,3]

1 Department of Radiology, Memorial Sloan-Kettering Cancer Center, New York, USA
2 Department of Materials Science and Engineering, Cornell University, New York, USA
3 Program in Molecular Pharmacology and Chemistry, Memorial Sloan-Kettering Cancer Center, New York, USA

DOE DE-SC0002184 09/01/09-08/31/11

Grant title: Multimodality Imaging with Silica-Based Targeted Nanoparticle Platforms

Abstract

Objectives: To synthesize and characterize a C-Dot silica-based nanoparticle containing "clickable" groups for the subsequent attachment of targeting moieties (e.g., peptides) and multiple contrast agents (e.g., radionuclides with high specific activity) [1,2]. These new constructs will be tested in suitable tumor models *in vitro* and *in vivo* to ensure maintenance of target-specificity and high specific activity.

Methods: Cy5 dye molecules are cross-linked to a silica precursor which is reacted to form a dye-rich core particle. This core is then encapsulated in a layer of pure silica to create the core-shell C-Dot (Figure 1) [2]. A 'click' chemistry approach has been used to functionalize the silica shell with radionuclides conferring high contrast and specific activity (*e.g.* 64Cu and 89Zr) and peptides for tumor targeting (*e.g.* cRGD and octreotate) [3]. Based on the selective Diels-Alder reaction between tetrazine and norbornene, the reaction is bioorthogonal, highyielding, rapid, and water-compatible. This radiolabeling approach has already been employed successfully with both short peptides (*e.g.* octreotate) and antibodies (*e.g.* trastuzumab) as model systems for the ultimate labeling of the nanoparticles [1].

Results: PEGylated C-Dots with a Cy5 core and labeled with tetrazine have been synthesized (d = 55 nm, zeta potential = -3 mV) reliably and reproducibly and have been shown to be stable under physiological conditions for up to 1 month. Characterization of the nanoparticles revealed that the immobilized Cy5 dye within the C-Dots exhibited fluorescence intensities over twice that of the fluorophore alone. The nanoparticles were successfully radiolabeled with Cu-64. Efforts toward the conjugation of targeting peptides (*e.g.* cRGD) are underway. *In vitro* stability, specificity, and uptake studies as well as *in vivo* imaging and biodistribution investigations will be presented.

Conclusions: C-Dot silica-based nanoparticles offer a robust, versatile, and multi-functional platform to enhance in vivo detection sensitivity and non-invasively assay receptor expression/status of tumor cellular targets, including those of low abundance, using nuclear-NIR

fluorescence imaging approaches [2]. Improvements in molecular diagnostics, refined by the availability of nanotechnology platforms, will be a key determinant in driving early-stage disease detection and prevention, ultimately leading to decreases in mortality.

Introduction and Background:

The original application was in response to the FOA "DE-PS02-09ER09-18; Radiochemistry" and studied radiochemistry, multimodality imaging technology, and nanoparticles. To improve detection of low abundance systems, characterization, and treatment monitoring of diseases, we sought to construct highly-specific, molecular-targeted probes, along with high-resolution imaging strategies. Here, we discuss new techniques for the labeling of silica-based nanoparticles with contrast agents for SPECT, PET CT, MRI, and optical imaging.

Hypothesis and Specific Aims:

The central hypothesis of this application was that *a robust and versatile silica-based nanoparticle platform could be functionalized to enhance in vivo detection sensitivity and non-invasively assay receptor expression/status of tumor cellular targets, including those of low abundance, using nuclear-NIR fluorescence imaging approaches.*

We addressed the following Specific Aims:

SA1. Design and synthesis of silica-based nanoparticles containing "clickable" groups for the subsequent attachment of targeting moieties (e.g., peptides) and multiple contrast agents (e.g., radionuclides with high specific activity).

SA2. Synthesis and physicochemical characterization of functionalized nanoparticles using model peptides and chelates.

SA3. *In vitro* and *in vivo* testing of these new constructs in suitable tumor models to ensure maintenance of target-specificity and high specific activity, as compared with the corresponding native radiolabeled peptides.

RESULTS

SA1. Design and synthesis of silica-based nanoparticles containing "clickable" groups for the subsequent attachment of targeting moieties (e.g., peptides) and multiple contrast agents (e.g., radionuclides with high specific activity). In order to optimize labeling conditions and synthesize an array of C-dot-peptide-chelate constructs, suitable for high-specific activity radiolabeling, we proposed to explore an approach to functionalizing the C-dot surface based on the inverse electron-demand Diels-Alder "click chemistry" ligation of tetrazine and the dienophile norbornene (Figures 1).

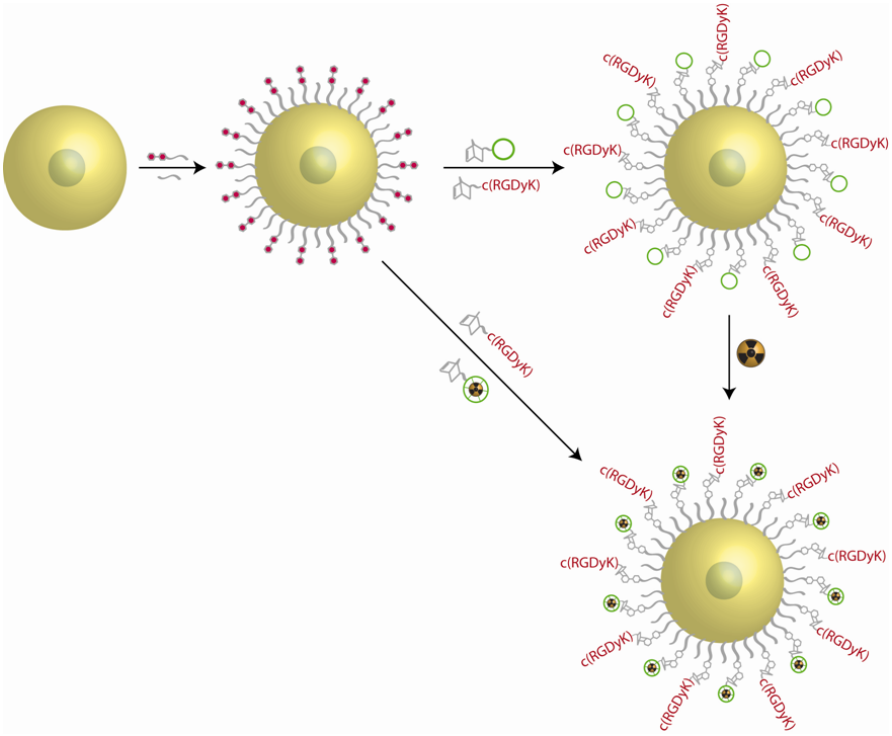

Figure 1. Stylized representation of the production of "clickable" C-dots with core-shell particle geometry containing the optical dye, Cy5. These C-dots have a fluorescent dye within their core and have a PEG surface-coating. Additionally they are decorated with tetrazine for subsequent "click" chemistry with both DFO and Tyr^3-octreotate functionalized with norbornene groups (SA2). We will be able to stockpile "clickable" C-dots that can be used for the desired multimodal application on any given day.

C-dot Synthesis and Characterization: PEG-ylated C-dots were synthesized by a modified Stöber-type silica condensation as previously described. Imaging was provided by SEM from Cornell University. PEG groups (Figure 2) were covalently attached as shown below (Figure 3). Bare particles were dialyzed to deionized water, and ethylene glycol-coated particles were dialyzed to physiological saline (0.15 M NaCl), through 3500 MWCO Snakeskin Dialysis Membranes (Pierce) and sterile-filtered through 0.2μm syringe filters. All samples were optical density-matched at their peak absorption wavelength (640 nm). Hydrodynamic size measurements were achieved by Dynamic Light Scattering (DLS) and Fluorescence Correlation Spectroscopy (FCS). Briefly, particles dialyzed to water were measured on a Brookhaven Instruments Company BIC 200SM static/dynamic light scattering system using a HeNe laser (λ = 632.8 nm). Due to overlap of the dye absorption with the excitation source, 15 minute integration times were used to achieve acceptable signal to noise ratios. For FCS, particles were dialyzed to water and diluted into physiological saline (0.15 M NaCl in H_2O) and measured on a homebuilt instrument using HeNe 633 nm excitation. Instruments were calibrated for size prior to all measurements (Figure 4).

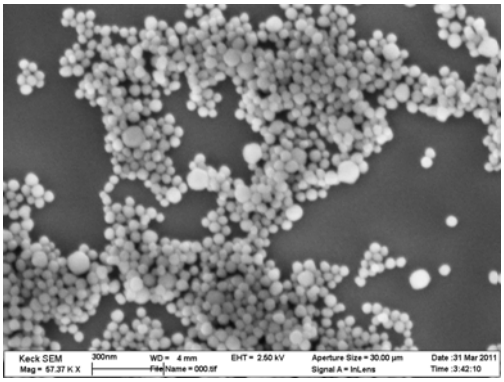

Figure 2. SEM image of 30 nm diameter C-dots.

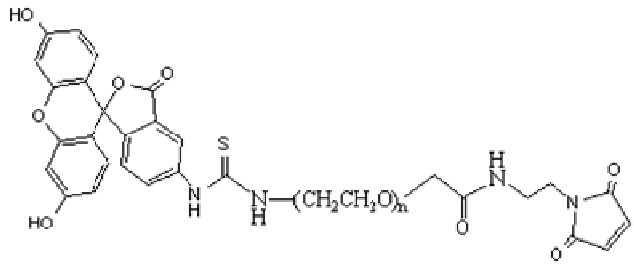

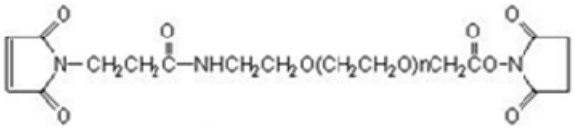

Figure 3. Structures of PEG derivatives. We used standard chemical pathways for the production of the functionalized PEG with tetrazine. These PEGs were covalently attached to the C-dot via the silane group. FITC dye and succinimide derivatives of maleimide-PEG are shown above and below, respectively.

Functionalization of C-dots with "Clickable" Groups: The synthesis of the bi-functionalized PEGs used commercially available reagents. The first step in this synthesis employed the well-studied tetrazine-based cycloaddition (Figure 4). Based on the selective Diels-Alder reaction between tetrazine and norbornene, the reaction is bioorthogonal, high-yielding, rapid, and water-compatible. This radiolabeling approach has already been employed successfully with both short peptides (e.g. octreotate) and antibodies (e.g. trastuzumab) as model systems for the eventual labeling of the nanoparticles.

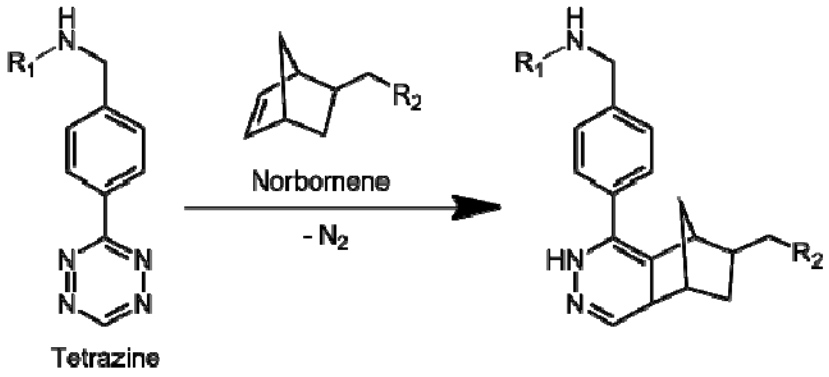

Figure 4. The inverse-electron demand Diels-Alder "click" ligation of benzylamino-tetrazine and linker-modified norbornene

The second step of the synthesis also relied on a well-known conjugation reaction. After the first reaction, the PEG chain should contain no reactive groups other than the activated bond, and we anticipated no side-products from this step either. After construction of the C-dot with the PEG, we quantified the number of average clickable groups by (1) using clickable "FITC" and (2) FTIR spectroscopy. We reacted this probe in excess to enable quantification of all of the available clicked bonds and then assayed using spectrofluorometry.

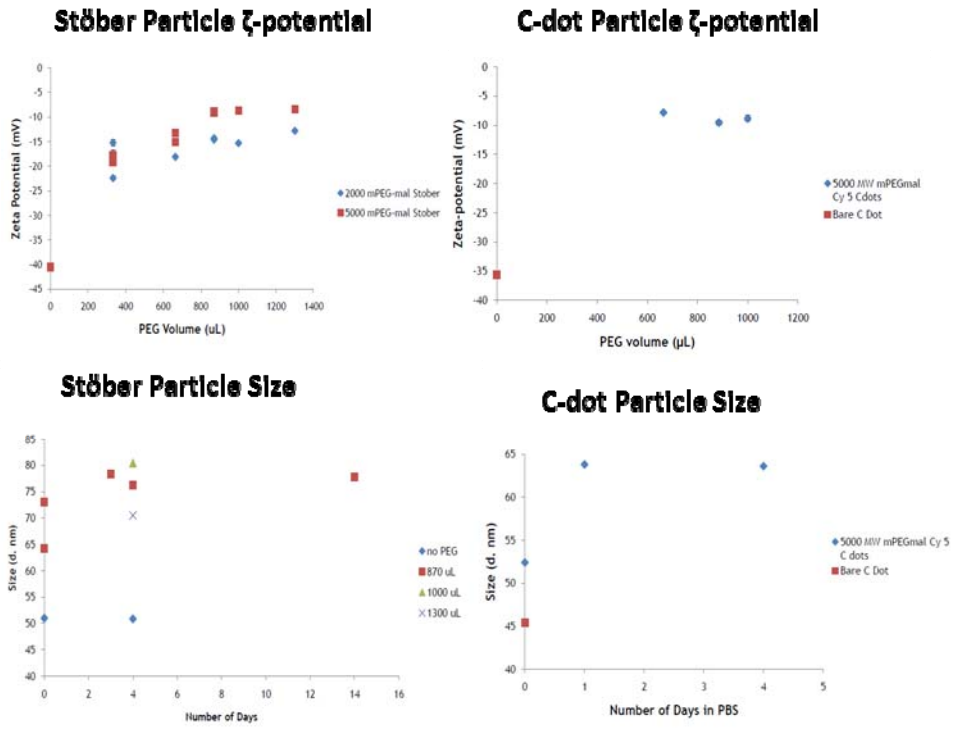

Figure 5. More PEG on nanoparticle surface increases zeta potential. Zeta potential plateaus at -7 mV, which is consistent with a calculated value of 3 PEG: 1 OH on the surface and indicates full surface coverage. PEGylated particles in PBS also show a size increase of about 10-15 nm when compared with non-PEGylated particles. Nanoparticles were stable for 4 weeks without size change.

SA2. Synthesis and physiochemical characterization of functionalized nanoparticles using model peptides and chelates. The ultimate goal was to prepare a versatile multimodality translatable materials platform for use in *in vitro* and *in vivo* radiochemistry applications. To do this, we explored the synthesis and characterization of functionalized "clickable" PEG-ylated C-dots containing both (A) a derivative of deferrioaxamine B (DFO) or 1,4,7,10-tetraazacyclododecane-1,4,7,10-tetraacetic acid (DOTA) for subsequent high-specific activity radiolabeling with the positron-emitting ^{89}Zr, and (B) the somatostatin receptor (SSTR)-targeting peptide, ocreotate (Figure 6). The combinations of these two systems acted as a model for the study of the C-dot platform.

Synthesis of "clickable" DFO and DOTA: We produced "clickable" DFO and DOTA with both the tetrazine and norbornene groups. This "clickable" DFO or DOTA was purified and fully characterized prior to attachment to the functionalized C-dots. We performed test reactions, where we used tetrazine contacting compound to "click" onto the DFO or DOTA to demonstrate the effectiveness of this approach and to optimize the reaction conditions prior to the attachment of the "clickable" chelators to the C-dots. The "click" reaction is a [4 + 2] Diels-Alder cycloaddition performed at room temperature.

Synthesis of "clickable" Tyr^3-octreotate: Solid phase peptide synthesis (SPPS) of Tyr^3-octreotate was performed on a peptide synthesizer from C S Bio Co. (Menlo Park, CA). The norbornene was introduced into the peptide backbone. This synthesis is capable of preparing large amounts for incorporation into the nanoparticles. The "clickable"-Tyr^3-octreotate was purified by reversed phase HPLC and purity and identity was determined by exact mass measurements using mass spectrometry. Cyclic-RGD was also supplied for conjugation to nanoparticles.

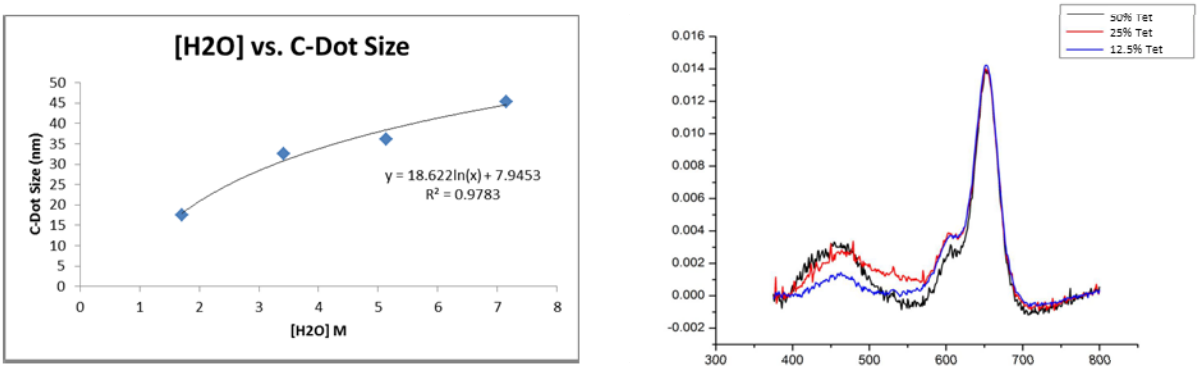

Figure 6. Adjusting synthesis parameters can alter particle morphology. For example, with increasing water concentration, larger particles can be synthesized that are uniformly sized and monodisperse. Increasing tetrazine concentration on the surface of the particle also changes the photophysical properties. UV-Vis analysis for tetrazine-coupled C-dots shows distinct peaks for the Cy5 dye and conjugated tetrazine.

Synthesis of functionalized C-dots: We have achieved the manufacture of three fully characterized pure components for construction of the functionalized C-dots:

(A) PEG-ylated C-dots with fluorescent Cy5 cores which are surface-modified with a known quantity of “clickable” groups.
(B) Desferrioxamine and DOTA-containing a tetrazine group – “clickable” DFO/DOTA
(C) Tyr^3-octreotate coupled to an azide-containing acid – “clickable” Tyr^3-octreotate

“Clickable” DOTA and “Clickable” Tyr^3-octreotate were reacted in known stoichiometry onto the C-dot (Table 1).

% PEG-Tetrazine	# Tetrazine per C-dot
0.8	<<1000
4.0	<<1000
10.0	~1000
12.5	~1000
20.0	~1000
25.0	~2000
50.0	~3000
100.0	~11000

Table 1. Increasing tetrazine concentration on the surface of the particle also changes the photophysical properties. This data shows that we can quantitate relative abundances of “clickable” groups.

We manufactured 30 nm type C-dots with up to 10^3 “clickable” groups *per* C-dot. As described above “click-labeling” is highly selective, quantitative and can be performed very fast and using mild conditions. “Clickable” DFO and “clickable” Tyr^3-octreotate can be added either simultaneously or sequentially to generate the required C-dot. Consideration should be made regarding yield and radiochemical purity for the synthesis route. The ratio of “clickable” DFO and “clickable” Tyr^3-octreotate was closely measured to create C-dots with DFO to Tyr^3-octreotate ratios of 1:1, 1:5, 1:10, 10:1, and 5:1.

Functionalized C-dot characterization: It was necessary to confirm the ratio of DFO chelates to Tyr^3-octreotate moieties on the PEG-ylated surface of the C-dot. We did already know, and confirmed, the C-dot concentration by FCS. Each entity still requires its own test to determine the *average* number per particle for quality control.

Average number of Tyr^3-octreotate peptide per C-dot: (A) the choice of Tyr^3-octreotate as a model peptide had one additional advantage, *the presence of a disulfide bridge*. The presence of this bridge allowed for quantification of the number of attached peptides to the C-dot on a small sample of product (Figure 7).The Measure-iT™ Thiol Assay Kit from Invitrogen was used. The assay had a linear range of 0.05-5 uM thiol, making it very sensitive. The assay was performed at room temperature; maximum signal was attained in 5 minutes and was stable for at least 1 hour.

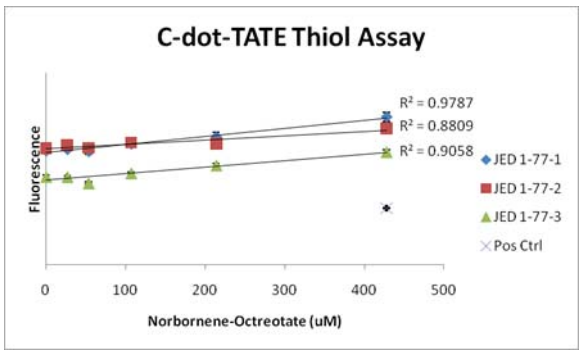

Figure 7. C-dots were functionalized with norbornene-octreotate. Increasing amounts of peptide added to particles could be detected and quantified using an Invitrogen Thiol Assay Kit. Particles with more tetrazine groups (JED 1-77-1, JED 1-77-2, and JED 1-77-3) conjugate more peptide.

SA3. *In vitro and in vivo* testing of these new constructs in suitable tumor models to ensure maintenance of target-specificity and high specific activity, as compared with the corresponding native radiolabeled peptides. The C-dot will allow for multivalency and production of high specific-activity agents which can target disease. This aim systematically explored the *in vitro* effects of ^{64}Cu-DOTA:octreotate stoichiometry on the C-dot to determine the optimal combination in regards to superior target affinity and localization (Figure 8). A lead compound with optimal ratios has recently been elucidated, and can be put forward for more intensive *in vivo* characterization. *In vivo* comparisons should also be made with the native ^{89}Zr-DFO-octreotide to demonstrate the increased targeting and accumulation we believe the C-dot platform will provide.

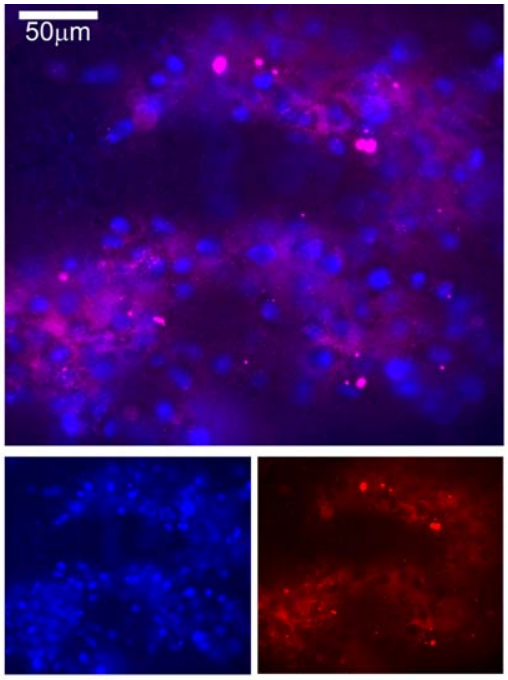

Figure 8. C-dots were found to internalize into the cytoplasm but did not localize in the nuclei (DAPI-blue, Cy5-red).

Radiochemistry: Initial radiolabeling of the DOTA-type C-dot conjugate was performed with ^{67}Ga and ^{64}Cu due the compatibility of these radionuclides with the DOTA chelator. The reaction was complete after less than 2 hours at room temperature. Non-specifically bound ^{67}Ga or ^{64}Cu was removed by addition of EDTA followed by a gel filtration step (representative ^{67}Ga radioTLC traces are shown in Figure 9). The goal was to achieve high-specific activity; therefore, optimal conditions were sought to ensure the highest labeling efficiency.

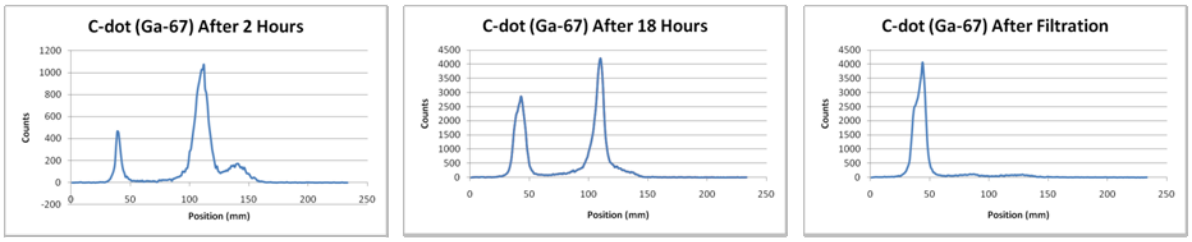

Figure 9. The nanoparticles were successfully radiolabeled with DOTA chelating Ga-67 or Cu-64. Instant Thin-Layer Chromatography (shown above) demonstrates >95% retention of Ga-67 on the C-dot nanoparticle. Centrifugal filtration is required to achieve radiochemically pure product. Particles with more tetrazine conjugated have higher labeling of the radioligand.

Receptor binding assays/in vitro assays: The receptor binding assays were performed using ^{64}Cu-DOTA-C-dots on membranes obtained from C6 glioma cells expressing SSTr2. Viability of cells and cell numbers were measured by trypan blue exclusion procedures using a hemocytometer. An aliquot of ~0.3 pmol of ^{64}Cu-DOTA-C-dots were added to 10 mL of cells, incubated at 37 °C with continuous agitation. At 1, 5, 15, 30, 45, 60 and 120 min triplicate 200-µL aliquots were removed and placed in ice. The cells were immediately isolated by centrifugation, and the % uptake of the compound into the cells was calculated (Figure 10).

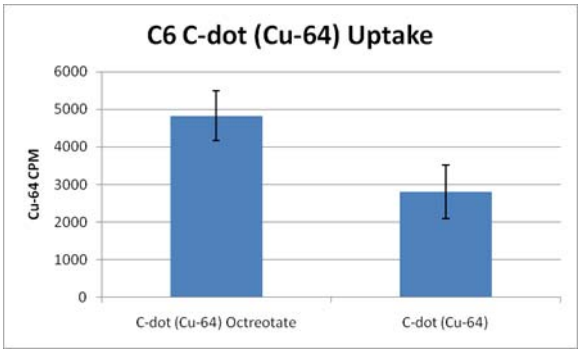

Figure 10. Octreotate particles labeled with DOTA-Cu-64 were targeted *in vitro* to C6 glioma cells expressing SSTr2. C-dots with peptide demonstrated over double the uptake in C6 cells when compared with C-dots lacking peptide.

In vivo NIRF imaging: Radiolabeled have yet to be injected intravenously into mice bearing palpable C6 glioma-positive tumors established in the xenograft model described previously. To date, only examinations of these particles lacking radionuclides has been attempted. To this end, serial fluorescence imaging was performed using the Maestro™ *In Vivo* Fluorescence Imaging System (CRI, Woburn, MA) at 0, 0.5, 1, 2, 4, 6, 12, 24, 48, and 72 hrs (Figure 11). From this data, is becomes apparent that the naked particle is preferentially taken up in the

spleen and gut of the mouse, though certainly targeting with a peptide will change this biodistribution.

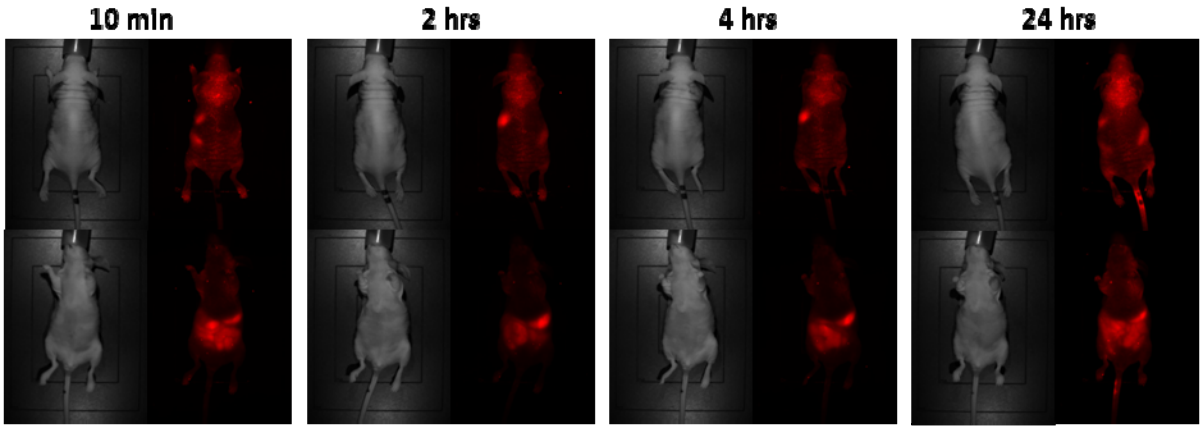

Figure 11. Examination of naked particle biodistribution in nude mice shows early uptake in spleen.

Results Summary:

Specific Aim 1: The C-dot manufacture is reproducible and did not cause any problems. We produced a novel "clickable" PEG construct for covalent attachment to the C-dot. This was done with commercially available chemicals using standard synthetic strategies.

Specific Aim 2: The chelator and peptide-modified C-dots were successfully constructed using inverse electron-demand Diels Alder click chemistry. "Clickable" norbornene-modified DFO and DOTA have been made in small scale reactions, and the norbornene-modified octreotate and cRGD peptides have been manufactured. Subsequently, the norbornene-modified chelators and peptides were reacted in known stoichiometry with the tetrazine-modified the C-dot. While characterization experiments confirmed the construction of the modified nanoparticle product and these results are very promising, conditions for construction can still be optimized further.

Specific Aim 3: While complete *in vitro* and *in vivo* experiments have yet to be performed, the complete nanoparticle construct has been prepared and stands ready for these experiments. The compound proposed to go into *in vivo* studies will be truly a multimodal platform and will allow us to examine the pharmacokinetics and pharmacodynamics of the C-dot constructs in animal models of cancer. The combined *in vitro* and *in vivo* data of this study will generate a wealth of information in the design and application of functionalized multimodality C-dots.

SUMMARY

We have synthesized and characterized a robust and versatile silica-based nanoparticle platform that can be functionalized to enhance *in vivo* detection sensitivity and non-invasively assay receptor expression/status of tumor cellular targets, including those of low abundance. By simultaneously optimizing design criteria, we have created a new generation of near-infrared fluorescent core-shell silica-based nanoparticles (C-dots). C-dots are non-toxic, highly

biocompatible, and offer a host of improved photophysical properties, including increased fluorescent efficiency and photostability. By exploring the use of a more generalizable modular approach, “click chemistry”, for functionalizing the fluorescent C-dots, we achieved a large range of chelate-peptide constructs for tumor targeting, as well as with radiolabels conferring higher contrast and specific activities. This C-dot architecture is readily translatable to other peptide and antibody systems, and other chelates such TETA and DTPA can be attached. These chelates can also be used to produce a myriad of PET, SPECT and MRI agents and therefore truly lead to multimodality imaging.

References:

[1] Burns *et al.*, (2006), Chem. Soc. Rev., 35, 1028-1042

[2] Ow *et al.*, (2005), Nano Letters, 5:1, 113-117

[3] Devaraj *et al.*, (2008), Bioconjugate Chem., 19, 2297-2299

[4] Lewis *et al.*, (1999), J. Med. Chem., 42, 1341-1347.

Clickable bifunctional radiometal chelates for peptide labeling†

Artem Y. Lebedev,[a] Jason P. Holland[a] and Jason S. Lewis*[ab]

Received (in Cambridge, UK) 25th November 2009, Accepted 26th January 2010
First published as an Advance Article on the web 6th February 2010
DOI: 10.1039/b924784j

Novel synthetic methods for producing an array of chelates for use in "click"-radiolabeling of peptides are described, and their reactivity with regards to subsequent conjugation and radiolabeling is discussed.

Standard techniques for radiolabeling of biomacromolecules use naturally occurring reactive groups which can result in the radionuclide being located at an unpredictable position on the molecule.[1] This lack of selectivity is particularly problematic in the case of peptides, because even subtle changes in the structure of a peptide can severely compromise its properties. The current solution for this problem is incorporation of the chelate into the peptide structure during the solid phase synthesis, before cleavage off the resin support and deprotection. This approach requires separate purifications for each synthesized conjugate and therefore complicates the synthesis of conjugate libraries. Conjugation chemistries such as the Huisgen cyclo-addition ("click" reaction) have recently been proposed as a suitable alternative.[2–5] Application of "click"-chemistry to peptide radiolabeling calls for convenient synthesis of "clickable" chelates for the radiometals.[6,7] Initial studies on the conjugation of the widely used 1,4,7,10-tetraazacyclododecane-1,4,7,10-tetraacetic acid (DOTA) to peptides *via* "click"-chemistry have been reported, but the value of this method was undermined by the complex (7 steps) synthetic procedures required to make the chelates and the long (12–18 hours) reaction times required for conjugation.[8] The full potential of ^{64}Cu-binding (^{64}Cu $t_{1/2}$ = 12.7 h, ideal for peptide labeling) chelates other than DOTA remain unexplored, despite the fact that 4,11-bis(carboxymethyl)-1,4,8,11-tetraazabicyclo[6.6.2]hexadecane (CB-TE2A) were demonstrated to be superior for use *in vivo*.[9] Desferrioxamine B (DFO), a ligand for radiolabeling with ^{68}Ga (1.1 h)[10] and ^{89}Zr (78.4 h),[11] has yet to be adopted to click-chemistry also.

We now report a streamlined synthetic approach to the "click" conjugation of chelates and peptides, along with selected members of the library of the "clickable" chelates. We also discuss how this particular conjugation method affects the radiolabeling of the resulting construct with ^{64}Cu.

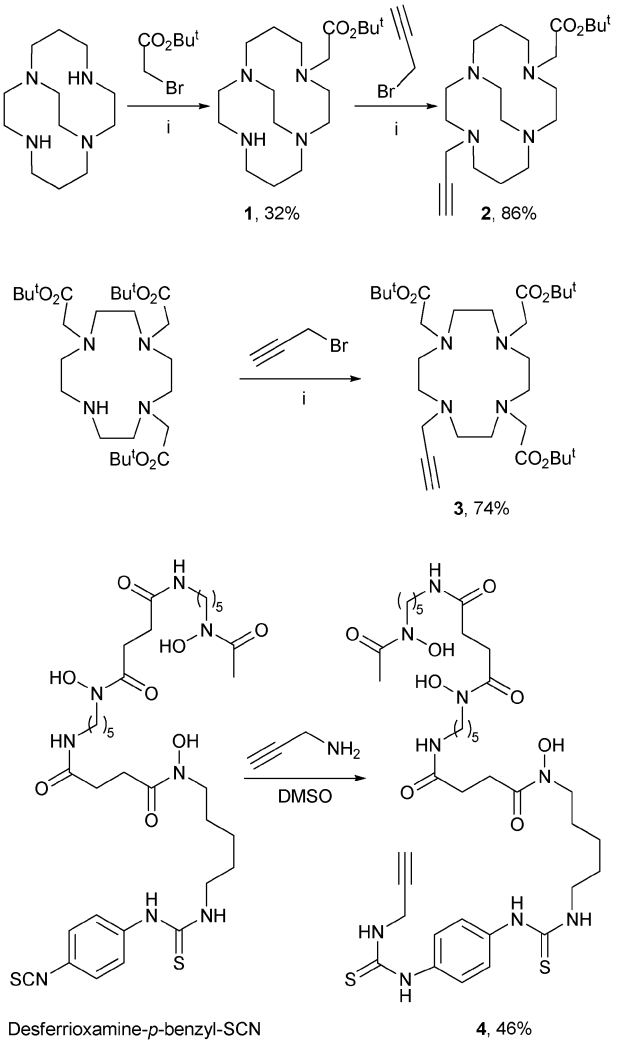

Scheme 1 Synthesis of the "clickable" chelates. (i) See ESI† for full details.

Scheme 1 illustrates the synthesis of the bifunctional chelators suitable for "click" conjugation. In order to avoid the formation of oligomers, only one reactive group should be present on the chelate. CB-TE2A was derivatised for use in the "click" reaction *via* a sequence of alkylation reactions. The first step involved reaction with protected bromoacetate,[12] followed by chromatographic isolation of the monoalkylated product **1**. The second reaction was performed by using similar conditions. This method afforded "clickable" CB-TE2A (**2**) reproducibly in around 80 to 90% yield. The DOTA analog **3** was synthesized in a similar manner. Commercial availability of monoactivated *p*-benzyl-SCN-DFO simplifies the synthesis

[a] *Radiochemistry Service, Department of Radiology, Memorial Sloan Kettering Cancer Center, 1275 York Avenue, New York, NY 10065, USA. E-mail: lewisj2@mskcc.org; Fax: +1 646 422 0408; Tel: +1 646 888 3038*
[b] *Program in Molecular Pharmacology and Chemistry, Memorial Sloan Kettering Cancer Center, 1275 York Avenue, New York, NY 10065, USA*

† Electronic supplementary information (ESI) available: Materials and methods, synthesis and radiolabeling, density functional theory (DFT) calculations, NMR and mass spectra, LC–MS profiles, radio HPLC profiles. See DOI: 10.1039/b924784j

of a respective "clickable" DFO analog. Simple reaction with propargyl amine yielded compound **4** in modest yield (46%) and isolation was achieved by using a C18 Sep-pak cartridge purification method common to radiochemistry.

The synthesized chelates were tested in "click" conjugation reactions involving a model peptide, which is known to target gastrin-releasing peptide receptors. The peptide was synthesized in accordance with standard Fmoc-protocols, and an azide-containing amino acid was coupled onto the N-terminus (see ESI† for details). Screening of the synthetic conditions for coupling the chelates to the peptide revealed that Cu^{+} formed *in situ* by reduction of $CuCl_2$ with ascorbic acid demonstrated the highest catalytic activity. Neither salts of Cu^{+} nor other reducing agents nor addition of triazole ligands[13] showed comparable activity. This system afforded quantitative conversion of the peptide **5** within 5 minutes at room temperature in aqueous solution. Quenching of the reaction with 0.01 M Na_2S (used to scavenge the copper catalyst) allowed for isolation of the metal-free conjugate using a C18 cartridge and the analytically pure sample was obtained after HPLC purification. Macrocyclic carboxyl groups were then deprotected with a TFA–iPr$_3$SiH–EDT cleavage cocktail. This protocol allowed the conjugation of both CB-TE2A and DOTA onto the model peptide (Scheme 2).

Preliminary radiolabeling experiments showed that both CB-TE2A and DOTA bearing constructs can be efficiently labeled with ^{64}Cu. At pH 6 in ammonium acetate buffer, the DOTA compound **6** forms the copper complex almost instantaneously. Radio-high performance liquid chromatography (HPLC) showed ~84% conversion (>95% purity after HPLC purification). The CB-TE2A conjugate (**7**) required heating for 5 min at 70 °C and after purification yielded radiolabeled conjugate of the same purity. To estimate the lower achievable limit of the specific activity we gradually increased the amount of ^{64}Cu added to the point of the peptide saturation. The specific activity of the radiolabeled conjugate can be as high as 250 mCi mg^{-1}. Experiments with non-radioactive Cu demonstrated the difference in retention time of the starting peptide and its copper derivative to be greater than 1 min for both chelators. Therefore, the specific activity of the HPLC purified product is primarily determined by the purity of the starting $^{64}CuCl_2$. The non-radioactive copper derivatives of **6** and **7** co-eluted with the respective radioactive compounds, confirming the identity of ^{64}Cu-**6** and ^{64}Cu-**7**.

The rate of the "click" reaction and the mild conditions of the radiolabeling are at odds with the previously published data. The peptide we employed as a model system for the click conjugation has been previously conjugated with CB-TE2A *via* the use of a conventional amide linker, but required harsh conditions for radiolabeling with ^{64}Cu up to 1.5 h at 95 °C.[14] Similarly, typical experimental conditions for the DOTA radiolabeling include heating at 50 to 65 °C.[15,16] This difference indicates that the triazole group is not an innocent linker, and suggests that there is an interaction between the lone pair of the azole ring and the metal ion. This interaction was not observed previously, because we are first to report the construct with a triazole group in the immediate vicinity of the copper ion. However, reports of triazole interaction with Tc do confirm the possibility of this interaction.[4] Coordination of copper with the chelating moiety could also facilitate the "click" reaction by bringing the catalyst in close proximity to the triple bond.

In the absence of a crystal structure, we conducted density functional theory (DFT) calculations in order to address whether the triazole ring of the copper labeled CB-TE2A "click" complex ^{64}Cu-**5** is capable of forming a coordinate bond to the Cu^{2+} ion.[17] Fig. 1 shows a picture of the DFT [uB3LYP/6-31+G(d,p)] optimized geometry of the model Cu complex **1** (see ESI† for full computational details and analysis).[10] The optimized metal-to-ligand bond lengths reveal that the complex is highly distorted and the elongated r(Cu–N7) bond length and r(Cu···N3) bonding interaction of 2.299

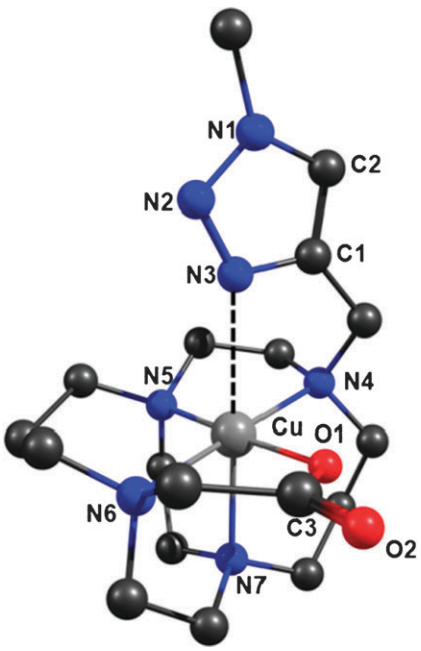

Fig. 1 DFT optimized structure of the hypothetical model complex. r(Cu···N3) = 2.559 Å; r(Cu–N4) = 2.110 Å; r(Cu–N5) = 2.092 Å; r(Cu–N7) = 2.299 Å; r(Cu–O1) = 1.930 Å.

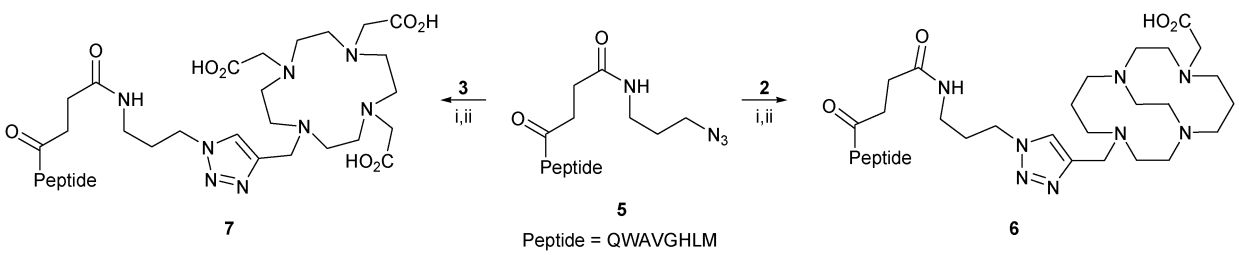

Scheme 2 "Click" conjugation onto the model peptide. (i) $CuCl_2$, ascorbic acid in water, RT; (ii) trifluoroacetic acid, iPr$_3$SiH, EDT.

and 2.559 Å, respectively, are consistent with the expected Jahn–Teller effects from the d^9 electron configuration.

Natural population analysis (NPA) correctly predicted a net positive charge on the Cu ion of 1.328e, and negative charges on all electronegative donor atoms (Table S1, ESI†). The nitrogen donor atoms N4–N7 of the CB-TE2A chelate have calculated NPA charges in the range −0.604 to −0.627e, and the donor oxygen atom has a net negative charge of −0.863e. Interestingly, the nitrogen atoms N1–N3 of the triazole ring show alternating NPA charges of −0.178, −0.068 and −0.338e, respectively. The negative NPA charge on nitrogen atom N3 is consistent with high electron density on this atom which facilitates a bonding interaction between the lone pair of electrons on atom N3 and the Cu^{2+} ion.

In order to ascertain if the Cu···N3 interaction constitutes a bond, natural bond orbital (NBO) analysis was used to investigate the nature and magnitude of the stabilizing interactions calculated within complex **1**. NBO analysis revealed that stabilizing orbital electron density interactions between the ligand donor atoms and the Cu^{2+} ion contribute 20.2% of the overall stability of complex **1**, of which 16.9% arises from ligand-to-metal donation and only 3.3% from metal-to-ligand back-bonding. The strongest bonding interaction occurs between the Cu^{2+} ion and the donor oxygen atom O1 with a total NBO interaction energy of 98 kcal mol^{-1} (5.3% of the total interaction). Interactions between the Cu^{2+} ion and the equatorial donor nitrogen atoms N4–N6 contribute between 62–66 kcal mol^{-1} each to the overall stability of complex **1**. Despite the shorter bond length of *r*(Cu–N7) of 2.299 Å compared to 2.559 Å from *r*(Cu···N3), NBO analysis indicates that the Cu···N3 bond (47 kcal mol^{-1}, 2.6% of the total NBO stabilization energy) is stronger than the Cu–N7 bond (35 kcal mol^{-1} [1.9%]). The additional stabilization energy for the Cu···N3 interaction arises due to an increased contribution from metal-to-ligand back-bonding which accounts for 26.8% of the total bonding interaction (Table S2, ESI†). In contrast, back-bonding only accounts for 16.6% of the Cu–N7 interaction. The strength of the Cu···N3 interaction is calculated to be equal to 49.0% of the strength of the Cu–O1 interaction and around 77.0% of the strength of the equatorial Cu–[N4–N6] interactions.

Molecular orbital (MO) analysis also reveals the origins for the difference in bond strength observed between the Cu–N7 and Cu···N3 bonds. The highest occupied molecular orbital (HOMO) in the β-spin manifold (βHOMO), and its α-spin spatial counterpart, the αHOMO−1, showed strong metal–ligand σ*-anti-boding interactions between the d_{z^2} orbital of the Cu^{2+} ion and pσ-orbitals of the donor nitrogen atoms N3 and N7 (Fig. S1, ESI†). The two spin orbitals show pronounced asymmetry with a larger MO coefficient from N7 atom and only a small contribution from the N3 donor. Differential orbital contributions from the N3 and N7 donor orbitals reduce the Cu–N7 bond order and weaken the bond to a greater extent than the Cu···N3 bond.

In summary, we have presented versatile methods for the synthesis of novel bifunctional chelates suitable for "click" conjugation to the peptides. "Click" conjugation of these molecules was demonstrated on a model peptide and the resulting conjugates have been labeled with ^{64}Cu, yielding radiolabeled constructs with high chemical purity and specific activity. In contrast to reported conditions for radiolabeling the complexation reaction between $^{64}Cu^{2+}$ and the CB-TE2A compound **4** was performed under mild conditions. This change in radiolabeling chemistry may be the result of additional interactions between the Cu^{2+} ion and the triazole ring. Further studies investigating the kinetics of radiolabeling and complex formation are underway.

We gratefully acknowledge the Office of Science (BER), U. S. Department of Energy (Awards DE-SC0002456 and DE-SC0002184), for funding. We thank Prof. Jennifer C. Green for access to computational facilities.

Notes and references

1 M. W. Brechbiel, *Q. J. Nucl. Med. Mol. Imaging*, 2008, **52**, 166–173.
2 A. J. de Graaf, M. Kooijman, W. E. Hennink and E. Mastrobattista, *Bioconjugate Chem.*, 2009, **20**, 1281–1295.
3 J. Marik and J. L. Sutcliffe, *Tetrahedron Lett.*, 2006, **47**, 6681–6684.
4 T. L. Mindt, H. Struthers, L. Brans, T. Anguelov, C. Schweinsberg, V. Maes, D. Tourwe and R. Schibli, *J. Am. Chem. Soc.*, 2006, **128**, 15096–15097.
5 T. L. Mindt, C. Muller, F. Stuker, J. F. Salazar, A. Hohn, T. Mueggler, M. Rudin and R. Schibli, *Bioconjugate Chem.*, 2009, **20**, 1940–1949.
6 H. Struthers, T. L. Mindt and R. Schibli, *Dalton Trans.*, 2010, **39**, 675–696.
7 C. J. Anderson and R. Ferdani, *Cancer Biother. Radiopharm.*, 2009, **24**, 379–393.
8 S. Knor, A. Modlinger, T. Poethko, M. Schottelius, H. J. Wester and H. Kessler, *Chem.–Eur. J.*, 2007, **13**, 6082–6090.
9 J. C. Garrison, T. L. Rold, G. L. Sieckman, S. D. Figueroa, W. A. Volkert, S. S. Jurisson and T. J. Hoffman, *J. Nucl. Med.*, 2007, **48**, 1327–1337.
10 P. M. Smithjones, B. Stolz, C. Bruns, R. Albert, H. W. Reist, R. Fridrich and H. R. Macke, *J. Nucl. Med.*, 1994, **35**, 317–325.
11 J. P. Holland, Y. C. Sheh and J. S. Lewis, *Nucl. Med. Biol.*, 2009, **36**, 729–739.
12 C. A. Boswell, C. A. S. Regino, K. E. Baidoo, K. J. Wong, A. Bumb, H. Xu, D. E. Milenic, J. A. Kelley, C. C. Lai and M. W. Brechbiel, *Bioconjugate Chem.*, 2008, **19**, 1476–1484.
13 Q. Wang, T. R. Chan, R. Hilgraf, V. V. Fokin, K. B. Sharpless and M. G. Finn, *J. Am. Chem. Soc.*, 2003, **125**, 3192–3193.
14 T. J. Wadas, M. Eiblmaier, A. Zheleznyak, C. D. Sherman, R. Ferdani, K. Liang, S. Achilefu and C. J. Anderson, *J. Nucl. Med.*, 2008, **49**, 1819–1827.
15 W. P. Li, J. S. Lewis, J. Kim, J. E. Bugaj, M. A. Johnson, J. L. Erion and C. J. Anderson, *Bioconjugate Chem.*, 2002, **13**, 721–728.
16 Z. Cheng, Z. M. Xiong, M. Subbarayan, X. Y. Chen and S. S. Gambhir, *Bioconjugate Chem.*, 2007, **18**, 765–772.
17 M. J. Frisch, *GAUSSIAN03*, Gaussian Inc., (see ESI† for the complete reference).

Bioconjugate Chemistry

ARTICLE

pubs.acs.org/bc

Modular Strategy for the Construction of Radiometalated Antibodies for Positron Emission Tomography Based on Inverse Electron Demand Diels−Alder Click Chemistry

Brian M. Zeglis,[†] Priya Mohindra,[†] Gabriel I. Weissmann,[†] Vadim Divilov,[†] Scott A. Hilderbrand,[‡] Ralph Weissleder,[‡] and Jason S. Lewis*[,†]

[†]Department of Radiology and the Program in Molecular Pharmacology and Chemistry, Memorial Sloan-Kettering Cancer Center, New York, New York, United States

[‡]Center for Systems Biology, Massachusetts General Hospital/Harvard Medical School, Boston, Massachusetts, United States

Supporting Information

ABSTRACT: A modular system for the construction of radiometalated antibodies was developed based on the bioorthogonal cycloaddition reaction between 3-(4-benzylamino)-1,2,4,5-tetrazine and the strained dienophile norbornene. The well-characterized, HER2-specific antibody trastuzumab and the positron emitting radioisotopes ^{64}Cu and ^{89}Zr were employed as a model system. The antibody was first covalently coupled to norbornene, and this stock of norbornene-modified antibody was then reacted with tetrazines bearing the chelators 1,4,7,10-tetraazacyclo-dodecane-1,4,7,10-tetraacetic acid (DOTA) or desferrioxamine (DFO) and subsequently radiometalated with ^{64}Cu and ^{89}Zr, respectively. The modification strategy is simple and robust, and the resultant radiometalated constructs were obtained in high specific activity (2.7−5.3 mCi/mg). For a given initial stoichiometric ratio of norbornene to antibody, the ^{64}Cu-DOTA- and ^{89}Zr-DFO-based probes were shown to be nearly identical in terms of stability, the number of chelates per antibody, and immunoreactivity (>93% in all cases). *In vivo* PET imaging and acute biodistribution experiments revealed significant, specific uptake of the ^{64}Cu- and ^{89}Zr-trastuzumab bioconjugates in HER2-positive BT-474 xenografts, with little background uptake in HER2-negative MDA-MB-468 xenografts or other tissues. This modular system—one in which the divergent point is a single covalently modified antibody stock that can be reacted selectively with various chelators—will allow for both greater versatility and more facile cross-comparisons in the development of antibody-based radiopharmaceuticals.

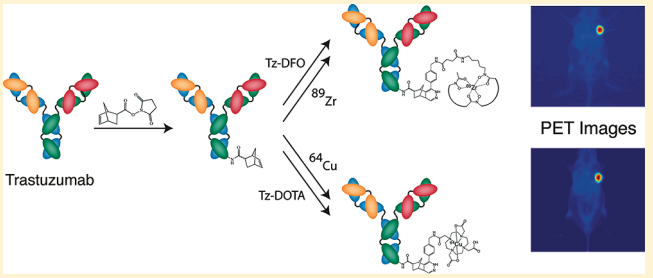

INTRODUCTION

Over the past two decades, radiopharmaceuticals based on antibodies have assumed an increasingly prominent role in both diagnostic and therapeutic nuclear medicine. This trend is particularly evident in the field of positron emission tomography (PET), in which a wide variety of effective antibody-based radiotracers have been developed against an array of cancer biomarkers.[1−3] Indeed, while some promising imaging agents have been labeled with long-lived nonmetallic radionuclides such as ^{124}I, the majority of antibody-based PET bioconjugates have employed positron-emitting radiometals, including ^{64}Cu, ^{86}Y, and, most recently, ^{89}Zr.[4−8] In these systems, radiometals offer significant advantages over their nonmetallic cousins, most notably decay characteristics that result in high image quality, radioactive half-lives that complement the biological half-lives of the antibody vectors, and enhanced control and ease of radiolabeling through the use of chelating moieties.

Despite their benefits, however, these chelating moieties are the source of a somewhat confounding issue in the study of radiometalated antibodies. Put simply, different radiometals require different chelators. For example, the small, hard $^{89}Zr^{4+}$ cation shows very high affinity for the multiple oxygen donors of the chelator desferrioxamine (DFO), while the larger and softer $^{64}Cu^{2+}$ cation exhibits higher thermodynamic and kinetic stability when bound to chelators bearing nitrogen donors in addition to oxygens, for example, 1,4,7,10-tetraazacyclo-dodecane-1,4,7,10-tetraacetic acid (DOTA) and 1,4,8,11-tetraazabicyclo[6.6.2]hexadecane-4,11-diyl)diacetic acid (CB-TE2A).[6,9] Further, different chelators often require dramatically different synthetic strategies for antibody couplings.[10] In an isolated case of one antibody and one radiometal, these facts do not present a problem. However, they do create a significant obstacle to the versatility of radiometalated bioconjugates. To wit, given a particular monoclonal antibody, the development of a ^{64}Cu-CB-TE2A-mAb conjugate for PET, a ^{89}Zr-DFO-mAb conjugate for PET, and a ^{225}Ac-DOTA-mAb conjugate for therapy would require three different routes

Received: June 4, 2011
Revised: August 22, 2011
Published: August 31, 2011

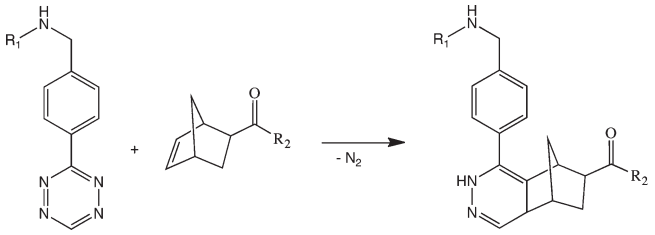

Figure 1. Tetrazine−norbornene ligation.

for antibody modification. Not only would this require additional time to develop and optimize each pathway, but the disparate routes would also mandate differing reaction conditions for each antibody, opening the door for differences in immunoreactivity and chelator/antibody ratio and ultimately making meaningful comparisons among the various radiopharmaceuticals more difficult. Consequently, a modular system—one in which the divergent point is a single covalently modified antibody stock that can be reacted selectively with various chelators—would resolve these issues and allow for more versatility and cross-comparisons in the development of antibody-based radiopharmaceuticals.

The chemical requirements of such a modular system—selectivity, biocompatibility, bioorthogonality—make it an almost perfect application for the use of click chemistry. Coined by K. Barry Sharpless, the term "click chemistry" broadly defines a group of chemical reactions by which two molecular components can be joined via a selective, rapid, clean, bioorthogonal, and biocompatible ligation.[11−13] By far, the most popular example of click chemistry is the Cu(I)-catalyzed [3 + 2] Huisgen cycloaddition between an azide and alkyne.[14] This reaction has already been widely employed in the development of radiotracers, particularly ^{18}F-based PET probes.[15−18] The application of this technology to radiometal-based probes has lagged behind, however, most likely due to concerns over metal contamination by the catalyst itself, though "clickable" chelators based on both the Cu(I)-catalyzed reaction and other Cu(I)-free systems have become more common in the literature in recent years.[19−22] Very recently, another promising "click" variant has come to light: the inverse electron demand Diels−Alder reaction between a tetrazine moiety and a strained alkene dienophile (Figure 1).[23−25] Like other click reactions, the ligation is selective, fast, biocompatible, and bioorthogonal, and unlike many Diels−Alder reactions, the coupling is irreversible, forming stable pyridazine products after the retro-Diels−Alder release of dinitrogen from the reaction intermediate. A number of different tetrazine-strained alkene pairs have been explored for the reaction, though the combination of 3-(4-benzylamino)-1,2,4,5-tetrazine (Tz) and either norbornene- or trans-cyclooctene-derivatives seems well-suited for biological applications. To date, the ligation has been employed in a variety of settings: the modification of oligonucleotides;[26] fluorescence imaging with small molecules, antibodies, and nanoparticles;[23,24,27,28] SPECT imaging with antibodies;[29] and ^{18}F-PET imaging with peptides.[30,31] However, to the best of the authors' knowledge, no application of this technology to positron-emitting radiometals has yet been made.

Herein, we report the development of a modular strategy for the construction of radiolabeled antibodies using the tetrazine-norbornene click reaction. The synthetic pathway involves three simple steps: (1) creation of a common stock of norbornene-modified antibody via peptide coupling; (2) ligation of a chelator-modified tetrazine moiety to the norbornene-modified antibody; and (3) radiolabeling of the resultant construct (Figure 2). For this proof of concept investigation, we have chosen the positron-emitting radiometals ^{64}Cu and ^{89}Zr, the chelators DOTA and DFO, and the antibody trastuzumab. ^{64}Cu and ^{89}Zr are the two most common radionuclides employed in antibody-based PET bioconjugates, and DOTA and DFO, respectively, are the most common chelators employed with these two metals.[6,9,10,32−34]

The antibody at hand, trastuzumab (Herceptin, Genentech), is an extremely well-characterized antibody specific to the human epidermal growth factor receptor 2 (HER2, also known as ERBB2). Overexpression of HER2 has been shown to be associated with augmented metastatic potential, increased tumor aggression, and poor prognosis for disease-free survival for patients with a variety of malignancies, most notably breast, ovarian, and colorectal cancer.[35−38] Trastuzumab alone has been employed as a therapeutic agent, and conjugates of both the antibody and its derivative fragments have been synthesized bearing a wide variety of radionuclides—including ^{64}Cu, ^{86}Y, ^{111}In, ^{124}I, ^{99m}Tc, and ^{89}Zr—for PET and SPECT imaging of HER2 expression.[39−47] It is our hope that this modular methodology will aid in both the expansion of the comparative study of antibodies labeled with different radionuclides and the development of novel antibody-based radiopharmaceuticals. Since more and more antibodies and dienophiles are being developed, this modular approach will likely lead to the rapid development of many novel imaging agents.[28] Importantly, while we have used positron-emitting radionuclides in this study due to our laboratory's area of expertise, this modular system need not be applied only to PET radiometals but rather can be used across the spectrum of metallic radionuclides, encompassing those employed for SPECT and radiotherapy as well.

EXPERIMENTAL PROCEDURES

Materials. All chemicals, unless otherwise noted, were acquired from Sigma-Aldrich (St. Louis, MO) and were used as received without further purification. All water employed was ultrapure (>18.2 MΩ cm^{-1} at 25 °C, Milli-Q, Millipore, Billerica, MA), and was passed through a 10 cm column of Chelex resin (Bio-Rad Laboratories, Hercules, CA) before use. DMSO was of molecular biology grade (>99.9%: Sigma, D8418), and all other solvents were of the highest grade commercially available. 1,4,7,10-Tetraazacyclododecane-1,4,7,10-tetraacetic acid mono-*N*-hydroxysuccinimidylester (DOTA-NHS) was purchased from Macrocyclics Inc. (Dallas, TX). *N*-Succinyldesferrioxamine B was prepared according to published procedures.[48] All instruments were calibrated and maintained in accordance with standard quality-control procedures.[49] UV−vis measurements were taken on a Cary 100 Bio UV−vis spectrophotometer. NMR spectroscopy was performed on a Bruker 500 MHz NMR with *Topsin 2.1* software for spectrum analysis. HPLC was performed using a Shimadzu HPLC equipped with a C-18 reversed-phase column (Phenomenex Luna analytical 4.6 × 250 mm or Semi-Prep 21.2 × 100 mm, 5 μm, 1.0 or 6.0 mL/min), 2 LC-10AT pumps, a SPD-M10AVP photodiode array detector, and a gradient of 0:100 MeCN/H_2O (both with 0.1% TFA) to 100:0 MeCN/H_2O over 15 min].

^{64}Cu was purchased from Washington University, St. Louis, where it was produced on the Washington University School of Medicine Cyclotron (model CS-15, Cyclotron Corp.) by the ^{64}Ni(p,n)^{64}Cu reaction and purified as previously described to

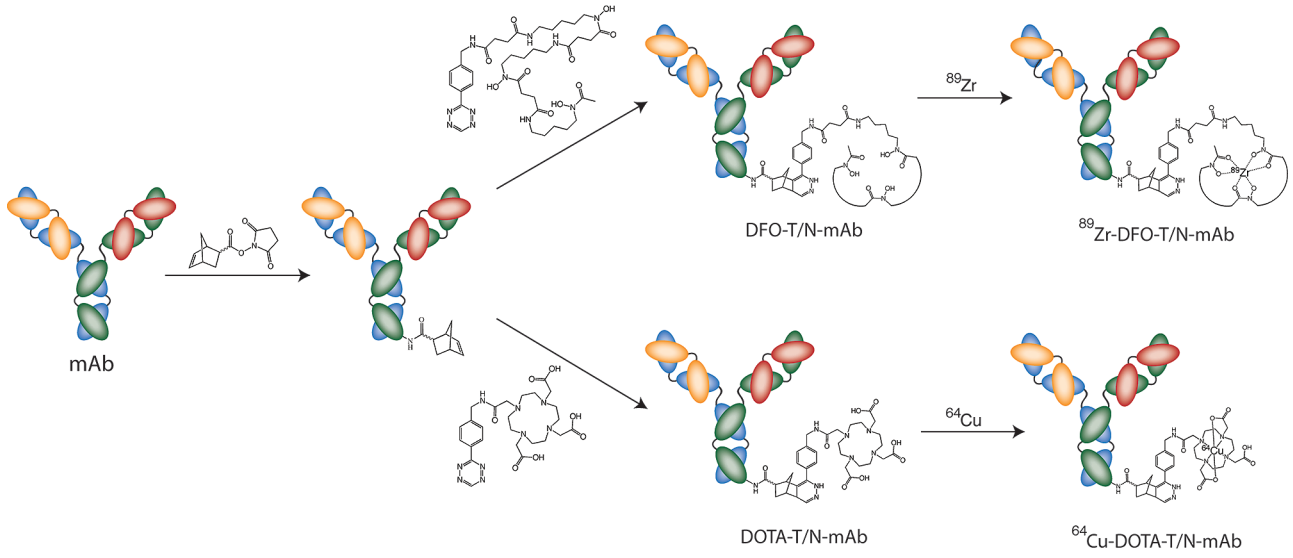

Figure 2. Schematic of a modular strategy for the construction of ^{89}Zr- and ^{64}Cu-modified antibody bioconjugates using the tetrazine-norbornene ligation.

yield [^{64}Cu]$CuCl_2$ with an effective specific activity of 200−400 mCi/μg (7.4−14.8 GBq/μg).[50] ^{89}Zr was produced at Memorial Sloan-Kettering Cancer Center on an EBCO TR19/9 variable-beam energy cyclotron (Ebco Industries Inc., British Columbia, Canada) via the ^{89}Y(p,n)^{89}Zr reaction and purified in accordance with previously reported methods to yield ^{89}Zr with a specific activity of 5.28−13.43 mCi/μg (195−497 MBq/μg).[51] All buffers used for ^{64}Cu and ^{89}Zr labeling were passed through Chelex resin before use. Activity measurements were made using a Capintec CRC-15R Dose Calibrator (Capintec, Ramsey, NJ). For accurate quantification of activities, experimental samples were counted for 1 min on a calibrated Perkin-Elmer (Waltham, MA) Automatic Wizard^2 Gamma Counter. Both ^{64}Cu and ^{89}Zr labeling reactions were monitored using silica-gel impregnated glass-fiber instant thin layer chromatography paper (Pall Corp., East Hills, NY) and analyzed on a Bioscan AR-2000 radio-TLC plate reader using Winscan Radio-TLC software (Bioscan Inc., Washington, DC). Human breast cancer cell lines BT-474 and MDA-MB-468 were obtained from the American Type Culture Collection (ATCC, Manassas, VA) and were grown by serial passage.

Synthesis of 3-(4-Benzylamino)-1,2,4,5-tetrazine (Tz). The protocol from Deveraj et al. was employed for the synthesis with slight modifications.[24] 4-(Aminomethyl)-benzonitrile hydrochloride (0.84 g, 0.005 mol) formamidine acetate (2.08 g, 0.02 mol), and elemental sulfur (0.16 g, 0.005 mol) were added to a dry, 50 mL round-bottom flask. Anhydrous hydrazine (2 mL) was then added to the flask, and the resultant orange reaction mixture was stirred for 20 h. After the allotted time, 1% $HCl_{(aq)}$ (50 mL) was slowly added to the reaction mixture, and the resultant solution was stirred for 10 min and subsequently filtered through a medium glass frit. The remaining orange solution was cooled in an ice bath to 0 °C, and a solution of 1.7 g of $NaNO_2$ in 15 mL of water was then added dropwise to the reaction mixture. While still cooled in an ice bath, acetic acid (50 mL) was added slowly, and the reaction mixture immediately turned bright pink. After allowing this solution to warm to room temperature over the course of 3 h, the solvent was evaporated at 50 °C and 20 Torr on a rotary evaporator. The resultant red crude solids were dissolved in 250 mL of water with 0.1% TFA. The aqueous solution was adsorbed onto a C_{18} column (Waters C_{18} Sep-Pak, Waters Corp., Milford, MA), washed with copious amounts of water, and eluted with acetonitrile. This bright pink, organic solution was evaporated to dryness, and the red crude was purified by flash chromatography (CombiFlash automated chromatography system, Teledyne Isco Inc., Lincoln, NE) using a gradient of 100% $CHCl_3$ (0.01% TFA) from 0 to 4 min followed by 0:100 MeOH (0.01%TFA)/$CHCl_3$ (0.01% TFA) to 30:70 (0.01%TFA)/HCl_3 (0.01% TFA) over 16 min. After the removal of solvent, the pure product was obtained in 35% yield (0.33 g, 0.0018 mol). ^{1}H NMR (500 MHz, D_2O), δ, ppm: 10.46 (s, 1H), 8.54 (d, 2H), 7.77 (d, 1H), 4.41 (s, 2H). ESI-MS: 188.1 $[M+H]^+$. HPLC t_R = 7.1 min.

Synthesis of N^1-(5-(4-((4-(1,2,4,5-Tetrazin-3-yl)benzyl)amino)-4-oxobutanamido)pentyl)-N^1-hydroxy-N^4-(5-(*N*-hydroxy-4-((5-(*N*-hydroxyacetamido)pentyl)amino)-4-oxobutanamido)pentyl)succinamide (Tz-DFO). 3-(4-Benzylamino)-1,2,4,5-tetrazine (8 mg, 0.045 mmol) was dissolved in DMSO (3 mL), and diisopropylethylamine (16 μL, 0.09 mmol) was added to this solution. After 15 min of stirring at RT, the pink DMSO solution was added to a second, premixed solution of *N*-succinyldesferrioxamine B (60 mg, 0.09 mmol) and benzotriazole-1-yl-oxy-tris-(dimethylamino)-phosphonium hexafluorophosphate (BOP, 53 mg, 0.12 mmol) in DMSO (3 mL). The combined reaction was stirred overnight and subsequently purified via C_{18} cartridge (Waters C_{18} Sep-Pak, Waters Corp., Milford, MA) and semipreparative reverse-phase HPLC. The purified product was obtained in 50% yield (molecular weight = 852.9, 19 mg, 0.023 mmol). ^{1}H NMR (500 MHz, DMSO-d_6), δ, ppm: 10.59 (s, 1H), 9.64 (s, 1H), 9.59 (s, 1H), 8.49 (m, 1H), 8.44 (d, 2H), 7.9−7.7 (m, 3H), 7.51 (d, 2H), 4.44 (d, 2H), 3.5−3.5 (m, 6H), 3.05−2.95 (m, 6H), 2.55 (t, 4H), 2.45−2.35 (m, 4H), 2.25 (t, 4H), 1.97 (s, 3H), 1.52−1.48 (m, 6H), 1.40−1.36 (m, 6H), 1.23−1.20 (m, 6H). ESI-MS: 831.5 $[M+H]^+$, 853.6 $[M+Na]^+$. HPLC t_R = 10.2 min.

Synthesis of 2,2′,2″-(10-(2-((4-(1,2,4,5-Tetrazin-3-yl)benzyl)amino)-2-oxoethyl)-1,4,7,10-tetraazacyclododecane-1,4,7-triyl)triacetic acid (Tz-DOTA). 3-(4-Benzylamino)-1,2,4,5-tetrazine (20 mg, 0.12 mmol) was dissolved in PBS (5 mL, pH 8.5), and diisopropylethylamine (40 μL, 0.24 mmol) was added

to this solution. This solution was then added to solid DOTA-NHS (50 mg, 0.065 mmol), and the resultant solution was stirred overnight at room temperature. The reaction was subsequently purified via C_{18} cartridge (Waters C_{18} Sep-Pak, Waters Corp., Milford, MA) and semipreparative reverse-phase HPLC. The purified product was obtained in 62% yield (molecular weight = 573.6, 23 mg, 0.04 mmol). ^{1}H NMR (500 MHz, DMSO-d_6), δ, ppm: 10.61 (s, 1H), 9.11 (br s, 1H), 8.50 (d, 2H), 7.62 (d, 2H), 4.50 (s, 2H), 4.42−4.38 (m, 4H), 3.65 (br s, 4H), 10.61 (s, 1H), 3.65−3.55 (m, 8H), 3.18−3.14 (m, 8H). ESI-MS: 574.5 $[M+H]^+$, 596.1 $[M+Na]^+$, 612.2 $[M+K]^+$. HPLC t_R = 8.1 min.

Antibody Modification. A protocol similar to that published by Devaraj et al. was employed for antibody modification.[24] 5-Norbornene-2-carboxylic acid (40 mg, 0.29 mmol) was incubated with 1.3 equiv of disuccinimidyl carbonate (100 mg, 0.39 mmol) and 1 equiv of pyridine (23 mg, 0.29 mmol) in dry acetonitrile (3 mL) for 2 h at room temperature. After 2 h, the solvent was removed via rotary evaporation, and the crude norbornene-succinimidyl ester product was recovered. Trastuzumab (purchased commercially as Herceptin, Genentech, San Francisco, CA) was purified using centrifugal filter units with a 30 000 molecular weight cutoff (Amicon Ultra 4 Centrifugal Filtration Units, Millipore Corp., Billerica, MA) and phosphate buffered saline (PBS, pH 7.4) to remove $\alpha-\alpha$-trehalose dihydrate, L-histidine, and polysorbate 20 additives. After purification, the antibody was taken up in PBS pH 8.0. Subsequently, 300 μL of antibody solution (150−250 μM) were combined with 100 μL PBS pH 8.0 and 1.5, 3, or 5 equiv of the crude norbornene-NHS ester in 10 μL of either DMF or DMSO. The reaction was incubated at room temperature for 2 h, followed by centrifugal filtration to purify the resultant antibody conjugate.

To perform the chelator ligation, 100 μL antibody solution (75−150 μM, PBS pH 7.4) was combined with 200 μL buffer (PBS pH 7.4) and a 10-fold molar excess of either Tz-DOTA or Tz-DFO in 10 μL DMSO (molar excess calculated based on initial norbornene reaction stoichiometry). The reaction was incubated at RT for 5 h and subsequently purified using centrifugal filtration to yield the completed DOTA- and DFO-modified antibodies. The final bioconjugates were stored in PBS pH 7.4 at 4 °C.

Labeling of DOTA-T/N-trastuzumab with ^{64}Cu. DOTA-T/N-trastuzumab (0.2−0.3 mg) was added to 200 μL labeling buffer (50 mM NH_4OAc, pH 5.5, though 50 mM NaOAc, pH 5.5 also is sufficient). $[^{64}Cu]CuCl_2$ (29.6−37 MBq, 800−1000 μCi) in approximately 1−3 μL 0.1 M HCl were then added to the antibody solution, and the resultant solution was incubated at room temperature for 1 h. After 1 h, the reaction progress was assayed using ITLC with an eluent of 50 mM EDTA, pH 5. The resultant ^{64}Cu-DOTA-T/N-trastuzumab was purified using either size-exclusion chromatography (Sephadex G-25 M, PD-10 column, 30 kDa, GE Healthcare; dead volume = 2.5 mL, eluted with 200 mL fractions of PBS, pH 7.4) or centrifugal column filtration. The radiochemical purity of the final radiolabeled bioconjugate was assayed by radio-TLC and was found to be >99% in all preparations. In the ITLC experiments, ^{64}Cu-DOTA-T/N-trastuzumab remains at the baseline, while $^{64}Cu^{2+}$ ions and $[^{64}Cu]$Cu-EDTA elute with the solvent front.

Labeling of DFO-T/N-trastuzumab with ^{89}Zr. DFO-T/N-trastuzumab (0.2−0.3 mg) was added to 200 μL buffer (PBS, pH 7.5). $[^{89}Zr]$Zr-oxalate (29.6−37 MBq, 800−1000 μCi) in 1.0 M oxalic acid was adjusted to pH 7.2−8.5 with 1.0 M Na_2CO_3. After evolution of CO_2(g) stops, the ^{89}Zr solution was added to the antibody solution, and the resultant mixture was incubated at room temperature for 1 h. After 1 h, the reaction progress was assayed using ITLC with an eluent of 50 mM EDTA, pH 5. The resultant ^{89}Zr-DFO-T/N-trastuzumab was purified using either size-exclusion chromatography (Sephadex G-25 M, PD-10 column, 30 kDa, GE Healthcare; dead volume = 2.5 mL, eluted with 200 mL fractions of PBS, pH 7.4) or centrifugal column filtration. The radiochemical purity of the final radiolabeled bioconjugate was assayed by radio-TLC and was found to be >99% in all preparations. In the ITLC experiments, ^{89}Zr-DFO-T/N-trastuzumab remains at the baseline, while $^{89}Zr^{4+}$ ions and $[^{89}Zr]$-EDTA elute with the solvent front.

Chelate Number. The number of accessible DFO and DOTA chelates conjugated to the antibodies was measured by radiometric isotopic dilution assays following methods similar to those described by Anderson et al. and Holland et al.[34,42,52,53] All experiments were performed in triplicate.

Immunoreactivity. The immunoreactivity of the ^{64}Cu-DOTA- and ^{89}Zr-DFO-T/N-trastuzumab bioconjugates was determined using specific radioactive cellular-binding assays following procedures derived from Lindmo et al.[54,55] To this end, BT-474 cells were suspended in microcentrifuge tubes at concentrations of 5.0, 4.0, 3.0, 2.5, 2.0, 1.5, and 1.0 × 10^6 cells/mL in 500 μL PBS (pH 7.4). Aliquots of either ^{64}Cu-DOTA- or ^{89}Zr-DFO-T/N-trastuzumab (50 μL of a stock solution of 10 μCi in 10 mL of 1% bovine serum albumin in PBS pH 7.4) were added to each tube (n = 4; final volume: 550 μL), and the samples were incubated on a mixer for 60 min at room temperature. The treated cells were then pelleted via centrifugation (3000 rpm for 5 min), resuspended, and washed twice with cold PBS before removing the supernatant and counting the activity associated with the cell pellet. The activity data were background-corrected and compared with the total number of counts in appropriate control samples. Immunoreactive fractions were determined by linear regression analysis of a plot of (total/bound) activity against (1/[normalized cell concentration]). No weighting was applied to the data, and data were obtained in triplicate.

Stability Measurements. The stability of the ^{64}Cu-DOTA- and ^{89}Zr-DFO-T/N-trastuzumab bioconjugates with respect to radiochemical purity and loss of radioactivity from the antibody was investigated *in vitro* by incubation of the antibodies in human serum for 48 h (^{64}Cu) or 7 d (^{89}Zr) at room temperature and 37 °C. The radiochemical purity of the antibodies was determined via radio-TLC with an eluent of 50 mM EDTA pH 5.0 (*vide supra*).

Cell Culture. Human breast cancer cell lines BT474 and MDA-MB-468 were obtained from the American Tissue Culture Collection (HTB-20 and HTB-132, respectively, ATCC, Bethesda, MD) and maintained in a 1:1 mixture of Dulbecco's Modified Eagle medium: F-12 medium, supplemented with 10% heat-inactivated fetal calf serum (Omega Scientific, Tarzana, Ca), 2.0 mM glutamine, nonessential amino acids, and 100 units/mL penicillin, and 100 units/mL streptomycin in a 37 °C environment containing 5% CO_2. Cell lines were harvested and passaged weekly using a formulation of 0.25% trypsin/0.53 mM EDTA in Hank's Buffered Salt Solution without calcium and magnesium.

Xenograft Models. All experiments were performed under an Institutional Animal Care and Use Committee-approved protocol, and the experiments followed institutional guidelines for the proper and humane use of animals in research. Six- to eight-week-old Athymic nu/nu female mice (NCRNU-M) were obtained from Taconic Farms Incorporated (Hudson, NY). Animals were

housed in ventilated cages, were given food and water *ad libitum*, and were allowed to acclimatize for approximately 1 week prior to treatment. Prior to tumor inoculation, mice were subcutaneously implanted with 0.72 mg 60 day release 17β-estradiol pellets (SE-121, Innovative Research of America, Sarasota, Florida) using a 10 gauge trocar. After several days, BT474 tumors were induced on the right shoulder by a subcutaneous injection of 3.0×10^6 cells in a 100 μL cell suspension of a 1:1 mixture of fresh media/BD Matrigel (BD Biosciences, Bedford, Ma). MDA-MB-468 tumors were induced on the left shoulder by a subcutaneous injection of 2.0×10^6 cells in the same manner (the number of cells injected was varied as described to compensate for cell growth rates and thus provide approximately the same tumor size at the time of radiopharmaceutical injection).

Acute Biodistribution. Acute *in vivo* biodistribution studies were performed in order to evaluate the uptake of the ^{64}Cu-DOTA- and ^{89}Zr-DFO-conjugated antibodies in mice bearing bilateral, subcutaneous BT-474 and MDA-MB-468 tumors (100−150 mm^3, 4 weeks postinoculation). Mice were randomized before the study and were warmed gently with a heat lamp for 5 min before administration of ^{64}Cu-DOTA-T/N-trastuzumab (0.74−1.11 MBq [20−30 μCi] in 200 μL 0.9% sterile saline) or ^{89}Zr-DFO-T/N-trastuzumab (0.56−0.74 MBq [15−20 μCi] in 200 μL 0.9% sterile saline) via intravenous tail vein injection (t = 0). Animals (n = 4 per group) were euthanized by CO_2(g) asphyxiation at 6, 12, 24, 36, 48, and 72 h (^{64}Cu) or 6, 24, 48, 72, 96, and 120 h (^{89}Zr). After asphyxiation, 13 organs (including both tumors) were removed, rinsed in water, dried in air for 5 min, weighed, and counted in a gamma counter calibrated for either ^{64}Cu or ^{89}Zr. Counts were converted into activity using a calibration curve generated from known standards. Count data were background- and decay-corrected to the time of injection, and the percent injected dose per gram (%ID/g) for each tissue sample was calculated by normalization to the total activity injected.

Small-Animal PET Imaging. PET imaging experiments were conducted on either a microPET Focus 120 (^{89}Zr) or a microPET R4 (^{64}Cu) rodent scanner (Concorde Microsystems).[56] Mice bearing bilateral, subcutaneous BT-474 (right shoulder) and MDA-MB-468 (left shoulder) tumors (100−150 mm^3, 4 weeks postinoculation) were administered ^{64}Cu-DOTA-T/N-trastuzumab (11.1−12.9 MBq [300−345 μCi] in 200 μL 0.9% sterile saline) or ^{89}Zr-DFO-T/N-trastuzumab (10.7−11.8 MBq [290−320 μCi] in 200 μL 0.9% sterile saline) via intravenous tail vein injection (t = 0). Approximately 5 min prior to the acquisition of PET images, mice were anesthetized by inhalation of 2% isoflurane (Baxter Healthcare, Deerfield, IL)/oxygen gas mixture and placed on the scanner bed; anesthesia was maintained using 1% isoflurane/gas mixture. PET data for each mouse were recorded via static scans at various time points between 6 and 120 h. A minimum of 20 million coincident events were recorded for each scan, which lasted between 10 and 45 min. An energy window of 350−700 keV and a coincidence timing window of 6 ns were used. Data were sorted into 2D histograms by Fourier rebinning, and transverse images were reconstructed by filtered back-projection (FBP) into a 128 × 128 × 63 (0.72 × 0.72 × 1.3 mm^3) matrix. The image data were normalized to correct for nonuniformity of response of the PET, dead-time count losses, positron branching ratio, and physical decay to the time of injection, but no attenuation, scatter, or partial-volume averaging correction was applied. The counting rates in the reconstructed images were converted to activity concentrations (percentage injected dose [%ID] per gram of tissue) by use of a system calibration factor derived from the imaging of a mouse-sized water-equivalent phantom containing ^{64}Cu or ^{89}Zr. Images were analyzed using *ASIPro VM* software (Concorde Microsystems).

Labeling Norbornene-Trastuzumab with [^{64}Cu]-Tz-DOTA. Tz-DOTA (5 μL of 1 mM solution in DMSO) was added to labeling buffer (50 mM NH_4OAc, pH 5.5), and [^{64}Cu]$CuCl_2$ (40.7−55.5 MBq [1100−1500 μCi]) in 0.1 M HCl were added to the reaction mixture. The resultant solution was incubated for 1 h at 85 °C, followed by purification via C_{18} cartridge (Waters C_{18} Sep-Pak, Waters Corp., Milford, MA) and radiochemical purity analysis via analytical HPLC (t_R = 10 min). The purified, radiolabeled [^{64}Cu]-Tz-DOTA was then added to a solution of norbornene-modified trastuzumab (0.4 mg, initial reaction stoichiometry of 5:1 norbornene/mAb) in PBS pH 7.4. The reaction mixture was allowed to incubate at 37 °C for 3 h. After 3 h, the progress of the reaction was assayed with radio-TLC using an eluent of 50 mm EDTA pH 5.0, and the radiolabeled antibody was purified with centrifugal filtration using centrifugal filter units with a 30 000 molecular weight cutoff (Amicon Ultra 4 Centrifugal Filtration Units, Millipore Corp., Billerica, MA) and phosphate buffered saline (PBS, pH 7.4). The radiochemical purity of the final radiolabeled bioconjugate was assayed again by radio-TLC and was found to be >99% in all preparations. In the radio-TLC experiments, ^{64}Cu-DOTA-T/N-trastuzumab remains at the baseline, while $^{64}Cu^{2+}$ ions, [^{64}Cu]Cu-Tz-DOTA, and [^{64}Cu]Cu-EDTA elute with the solvent front.

Statistical Analysis. Data were analyzed by the unpaired, two-tailed Student's t test. Differences at the 95% confidence level ($P < 0.05$) were considered to be statistically significant.

RESULTS AND DISCUSSION

Chemical Synthesis. 3-(4-Benzylamino)-1,2,4,5-tetrazine (Tz) was successfully synthesized through the reaction of 4-(aminomethyl)-benzonitrile hydrochloride, formamidine acetate, and elemental sulfur to form a dihydrotetrazine intermediate ((4-(1,2-dihydro-1,2,4,5-tetrazin-3-yl)phenyl)methanamine), followed by oxidation with $NaNO_2$ to form the aromatic tetrazine product. A method similar to that published by Devaraj et al. was employed; however, a number of small changes—for example, the use of 1% $HCl_{(aq)}$ rather than acetic acid in an intermediate step—were made and were found to considerably raise yields from the reported 20% to 35−40%. The product was characterized via UV−vis, ^{1}H NMR, ^{13}C NMR, and ESI-MS, and all data match that described in the original synthetic report.[24] Given the particularly promising nature of this cycloaddition reaction, the optimization of this synthesis was an important task. Tz was chosen as the particular tetrazine-based moiety for this line of experimentation due to its convenient, primary-amine coupling handle and its balance of reactivity and stability. To be sure, other tetrazine-based molecules with possible conjugation sites exist, but water instability (dimethyl 1,2,4,5-tetrazine-3,6-dicarboxylate), poor reactivity (1,2,4,5-tetrazine-3,6-diamine or 3,6-bis-(4-aminophenyl)-1,2,4,5-tetrazine), or instability (6-(6-(pyridin-2-yl)-1,2-dihydro-1,2,4,5-tetrazin-3-yl)pyridin-3-amine) render them unsuitable to the development of a modular system such as this.[29,57−59] Tz-DOTA and Tz-DFO (Scheme 1) were synthesized from Tz via simple peptide coupling reactions using the commercially available mono-NHS-ester of DOTA or *N*-succinyldesferrioxamine B and benzotriazole-1-yl-oxy-tris-(dimethylamino)-phosphonium hexafluorophosphate (BOP), respectively.

Scheme 1. Synthetic Route to Tz-DOTA and Tz-DFO

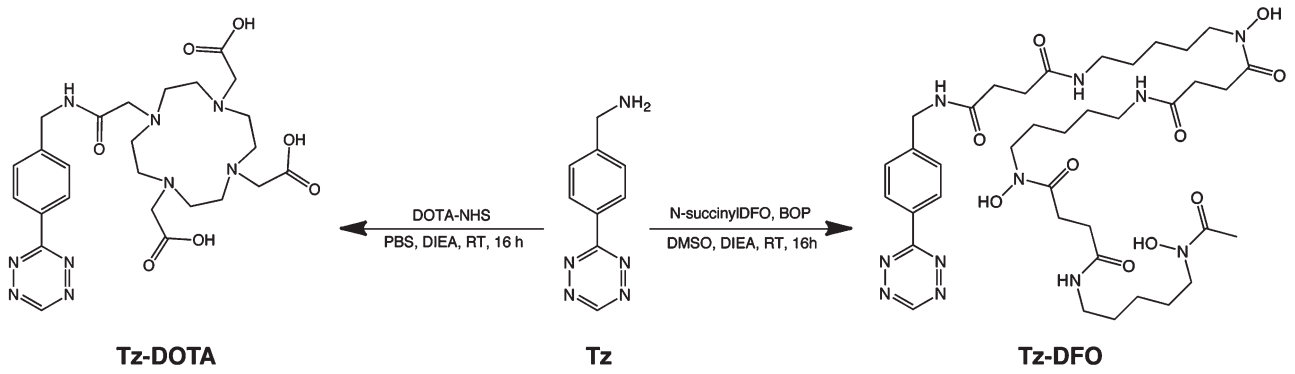

Table 1. Chemical and Biological Characterization Data for ^{64}Cu-DOTA-T/N- and ^{89}Zr-DFO-T/N-trastuzumab Bioconjugates

radionuclide	chelator	initial Nor/mAb reaction stoichiometry	chelates/mAb[a]	specific activity (mCi/mg)	immunoreactive fraction[b]	stability[c]
^{64}Cu	DOTA	1.5	1.0 ± 0.2	3.2 ± 0.4	0.96 ± 0.05	>98%
		3	2.3 ± 0.4	3.1 ± 0.2	0.95 ± 0.03	>96%
		5	3.7 ± 0.7	5.3 ± 0.5	0.94 ± 0.02	>96%
^{89}Zr	DFO	1.5	1.1 ± 0.3	2.7 ± 0.2	0.96 ± 0.03	>98%
		3	2.2 ± 0.3	2.9 ± 0.3	0.96 ± 0.04	>98%
		5	3.8 ± 0.9	4.3 ± 0.4	0.93 ± 0.05	>97%

[a] $n = 3$ for all experiments presented. [b] Determined prior to *in vivo* experimentation. [c] Calculated for incubation in human serum at 37 °C for 48 h (Cu) or 7 d (Zr).

Upon synthesis, both molecules were purified via reversed-phase HPLC and fully characterized by UV−vis, ^{1}H NMR, ^{13}C NMR, and ESI-MS. Importantly, Tz-DOTA exhibits high water solubility, but Tz-DFO does not. Consequently, DMSO was used as the stock solvent and delivery vehicle for both Tz-DOTA and Tz-DFO throughout the investigation in order to ensure that the antibodies in different branches of the modular pathway were exposed to exactly the same reaction conditions. Indeed, given the ease of synthesis of both Tz-DOTA and Tz-DFO, it is easy to envision the creation of a complete library of tetrazine-modified chelators—ranging from Tz-AmBaSar to Tz-HBED to Tz-DTPA—in order to maximize the utility and versatility of this modular construction strategy.

Antibody Modification, Radiolabeling, and Characterization. The radiolabeled trastuzumab bioconjugates were constructed via a modular three-step procedure (Figure 2). A common stock of norbornene-modified mAb was first produced via the room-temperature aqueous coupling of an NHS-ester of 5-norbornene-2-carboxylic acid with the exposed lysines of trastuzumab. After purification, the resultant norbornene-modified antibodies were then incubated for 5 h at room temperature with a 10-fold excess (based on norbornene loading) of the appropriate tetrazine-modified chelator—Tz-DOTA for ^{64}Cu or Tz-DFO for ^{89}Zr—and purified via centrifugal filtration or size exclusion chromatography. The bioconjugates were radiometalated with ^{64}Cu or ^{89}Zr at room temperature under either acidic (pH 5.5) or basic (pH 7.2−8.5) conditions, respectively. The crude radiochemical yields varied according to the initial norbornene loading of the antibody; however, after purification via centrifugal filtration, the ^{64}Cu-DOTA- or ^{89}Zr-DFO-T/N-trastuzumab conjugates were isolated with RCP >99% ($n = 3$ for each construct). The modification and radiolabeling strategy is simple, robust, and relatively rapid, and no antibody aggregation or precipitation issues were observed. Unlike other methods for the modification of mAbs with DOTA or DFO, overnight incubations, wide swings in buffer pH, and temperatures over room temperature are not required.[60−64] Importantly, we also observed that the tetrazine-norbornene ligation and subsequent radiolabeling proceeded almost identically whether performed the day of norbornene modification of the antibody or four weeks later (and likely after much longer periods of time, provided the antibody is stored at 4 °C). The radiolabeling of the DOTA- and DFO-modified trastuzumab conjugates is likewise robust, with the reaction providing similar yields with freshly prepared or four-week-old mAbs.

A number of chemical and *in vitro* tests were performed in order to characterize the chelator-modified and radiolabeled antibody constructs. Three different initial reaction stoichiometries of norbornene:mAb—1.5:1, 3:1, and 5:1—were employed to investigate the effect of different chelator loadings on the performance of the antibody. After the ligation of the variably norbornene-loaded antibodies with either Tz-DOTA or Tz-DFO, radiometric isotopic dilution experiments were performed in order to determine the number of accessible chelates on each antibody. The results, shown in Table 1, clearly illustrate that increasing initial loadings of norbonene result in higher numbers of chelates per antibody. Given the quantitative nature of the tetrazine/norbornene ligation and the proximity of the number of chelates per antibody to the initial modification stoichiometry in each case, calculating the loading of norbornenes per antibody was deemed unnecessary. The combined yield of the modification and ligation reactions is relatively consistent across all three

stoichiometries (~40−60%), and the results are generally consistent with antibody ligations using tetrazine/dienophile pairs reported by Devaraj et al., Haun et al., and Rossin et al.[23,28,29] Just as importantly, the number of chelates per antibody is, within error, identical for both the DOTA-T/N-trastuzumab and DFO-T/N-trastuzumab conjugates, a critical facet for such a modular system. Not surprisingly, the varying chelate numbers also played a role in the specific activities obtained for each antibody. All of the antibody conjugates were labeled in high specific activity (>2.0 mCi/mg). Interestingly, the specific activities of both the ^{64}Cu-DOTA-T/N-trastuzumab and ^{89}Zr-DFO-T/N-trastuzumab conjugates only roughly correlate with the number of chelates per antibody: those for ^{64}Cu-DOTA-T/N-trastuzumab range from 3.2 ± 0.4 mCi/mg to 5.3 ± 0.5 mCi/mg, though the specific activities for bioconjugates with initial nor/mAb ratios of 1.5:1 and 3:1 are within error of each other. Similarly, the specific activities of the ^{89}Zr-DFO-T/N-trastuzumab conjugates range from 2.7 ± 0.2 mCi/mg to 4.3 ± 0.4 mCi/mg, but again, the specific activities of the two conjugates with fewer DFO/mAb are statistically identical. Given the different specific activities of the original radiometals, comparisons between the specific activities of the two types of construct have little merit; however, the specific activities obtained in this investigation are consistent with those reported for other ^{64}Cu-DOTA-based and ^{89}Zr-DFO-based antibody bioconjugates in the literature.[6,10,34,42,45]

The immunoreactive fractions of the ^{64}Cu-DOTA- and ^{89}Zr-DFO-conjugates were determined via specific *in vitro* cellular association assays using the HER2/*neu* positive BT-474 breast cancer cell line.[54] Regardless of the number of chelates per antibody, all six conjugates exhibited immunoreactive fractions greater than 0.93 (n = 3 for each radiolabeled antibody). Blocking experiments performed with the addition of a vast excess (>500-fold) of unlabeled trastuzumab showed virtually no radioactive antibody binding and thus demonstrated the specificity of the ^{64}Cu-DOTA- and ^{89}Zr-DFO-T/N-trastuzumab. To assay the stability of radiolabeled bioconjugates, the ^{64}Cu-DOTA- and ^{89}Zr-DFO-T/N-trastuzumab formulations were incubated in human serum for 48 h and 7 d, respectively. Radio-TLC with an eluent of 50 mM EDTA (pH 5.0) illustrated that both sets of conjugates were >96% stable after the incubation period in all cases (Table 1).

Acute Biodistribution Studies. Acute biodistribution experiments and small animal PET imaging were performed in order to assay the *in vivo* efficacy of the ^{64}Cu and ^{89}Zr-bioconjugates. For all *in vivo* investigations, the trastuzumab bioconjugates with an initial nor/mAb stoichiometry of 5:1 were chosen, though similar results would be expected for all three ratios given the uniformly high immunoreactivity, stability, and specific activity observed in all of the constructs. In the biodistrubution experiment, nude mice bearing bilateral BT-474 (HER2-positive) and MDA-MB-468 (HER2-negative) were injected via tail vein with either ^{64}Cu-DOTA-T/N-trastuzumab (0.74−1.11 MBq [20−30 μCi] in 200 μL 0.9% sterile saline, specific activity: 5.1 mCi/mg) or ^{89}Zr-DFO-T/N-trastuzumab (0.56−0.74 MBq [15−20 μCi] in 200 μL 0.9% sterile saline, specific activity: 4.7 mCi/mg). Animals (n = 4 for each time point) were euthanized by CO_2(g) asphyxiation at 6, 12, 24, 36, 48, and 72 h (^{64}Cu) or 6, 24, 48, 72, 96, and 120 h (^{89}Zr). The organs (including tumors) of each animal were harvested and weighed, the amount of activity in each was counted on a gamma counter, and the %ID/g for each organ was calculated.

Table 2. Biodistribution Data of ^{64}Cu-DOTA-T/N-trastuzumab versus Time in Mice Bearing Bilateral s.c. BT-474 (HER2-positive) and MDA-MB-468 (HER2-negative) Xenografts (n = 4 for Each Time Point)

	6 h	12 h	24 h	48 h	72 h
blood	19.2 ± 5.2	16.2 ± 4.1	10.5 ± 3.6	11.2 ± 1.6	11.8 ± 1.3
HER2+ tumor	10.4 ± 4.6	23.9 ± 4.6	26.1 ± 4.8	44.0 ± 7.7	55.1 ± 2.3
HER2- tumor	6.2 ± 1.1	8.6 ± 2.7	9.0 ± 0.9	8.7 ± 2.5	11.7 ± 1.3
heart	4.9 ± 1.1	6.7 ± 2.7	4.3 ± 0.8	4.3 ± 1.2	5.7 ± 3.1
lungs	12.2 ± 1.2	9.5 ± 1.5	6.4 ± 2.3	8.0 ± 1.3	9.5 ± 0.4
liver	11.5 ± 2.0	10.1 ± 0.4	9.7 ± 1.3	6.4 ± 0.2	8.1 ± 0.9
spleen	11.1 ± 5.5	10.1 ± 1.4	10.6 ± 2.3	5.7 ± 0.4	6.9 ± 1.4
stomach	1.9 ± 0.7	1.0 ± 0.4	2.4 ± 0.3	1.3 ± 0.3	1.8 ± 0.2
sm intestine	3.5 ± 1.5	2.1 ± 0.3	3.5 ± 1.6	2.2 ± 0.1	2.6 ± 0.1
lg intestine	2.0 ± 0.3	1.7 ± 0.1	3.1 ± 1.7	1.4 ± 0.3	2.0 ± 0.4
kidney	5.5 ± 0.9	4.9 ± 1.0	2.9 ± 1.6	4.0 ± 0.4	4.5 ± 0.4
muscle	0.6 ± 0.2	0.7 ± 0.4	0.6 ± 0.3	1.0 ± 0.2	0.8 ± 0.1
bone	3.1 ± 2.7	1.4 ± 0.1	3.6 ± 0.4	1.1 ± 0.2	2.6 ± 1.1

In the ^{64}Cu-DOTA-T/N-trastuzumab biodistribution experiment (Table 2), high specific uptake is observed in the HER2-positive BT-474 tumor, with the %ID/g increasing from 10.4 ± 4.6 at 6 h to 55.1 ± 2.3 at 72 h (tumor/muscle ratios of 17.3 ± 7.1 and 68.8 ± 8.0, respectively). By comparison, far lower levels of ^{64}Cu-DOTA-T/N-trastuzumab uptake were seen in the HER2-negative MDA-MB-468 tumors. As expected, over the course of the experiment a concomitant decrease in the %ID/g in the blood (from 19.2 ± 5.2 at 6 h to 11.8 ± 1.3 at 72 h) also occurred. The organs with the highest background uptake were the lungs, liver, and spleen, though the uptake in these organs was at its highest point at 6 h, and by 72 h, the tumor/organ ratios for each of these organs were 5.8 ± 0.3, 6.8 ± 0.8, and 8.0 ± 1.6, respectively (see Supporting Information for complete table of tumor/organ ratios). Low levels of uptake were observed in the heart, stomach, small intestine, large intestine, kidney, muscle, and bone. Taken together, these results plainly indicate that ^{64}Cu-DOTA-T/N-trastuzumab is an effective imaging agent for the delineation of the HER2-positive BT-474 xenografts. Perhaps just as importantly, these results are consistent with those previously reported for ^{64}Cu-DOTA-T/N-trastuzumab conjugates, though the literature investigation used HER2-positive and HER2-negative non-small cell lung cancer cell lines.[65] Interestingly, far lower background liver uptake was observed in our study, and while comparisons between different tumor models systems may bear some risks, this discrepancy suggests a lower rate of ^{64}Cu decomplexation in our system.

Similarly positive results were observed in the ^{89}Zr-DFO-T/N-trastuzumab biodistribution experiments (Table 3). Initially very high blood activity levels decreased over the course of the experiment, from 42.2 ± 8.8%ID/g at 6 h to 18.2 ± 3.3%ID/g at 120 h. More importantly, high specific uptake was observed in the HER2-positive BT474 tumors, peaking at over 75%ID/g at 72 h postinjection (tumor to muscle ratio: 34.1 ± 12.7). In contrast, the uptake in the HER2-negative MDA-MB-468 tumors was significantly lower, starting at 11.2 ± 5.80%ID/g at 6 h and peaking at 120 h at 17.6 ± 3.9%ID/g. Highest background uptake was observed in the lungs, liver, spleen, and kidney, with uptake values ranging from 7 to 17%ID/g and typically decreasing over the course of the experiment. Maximum tumor to organ

Table 3. Biodistribution Data of ^{89}Zr-DFO-T/N-trastuzumab versus Time in Mice Bearing Bilateral s.c. BT-474 (HER2-positive) and MDA-MB-468 (HER2-negative) Xenografts (n = 4 for Each Time Point)

	6 h	24 h	48 h	72 h	96 h	120 h
blood	42.2 ± 8.8	37.4 ± 3.4	24.1 ± 6.1	24.1 ± 8.2	20.2 ± 2.1	18.2 ± 3.3
HER2+ tumor	22.9 ± 6.6	48.6 ± 6.9	64.0 ± 6.8	75.1 ± 7.6	72.2 ± 7.9	69.8 ± 3.9
HER2- tumor	11.2 ± 5.0	13.4 ± 4.1	14.5 ± 8.8	16.8 ± 2.7	16.7 ± 6.8	17.6 ± 1.7
heart	24.1 ± 5.7	17.7 ± 6.9	6.0 ± 3.2	9.6 ± 3.8	8.5 ± 3.2	10.4 ± 0.9
lungs	15.5 ± 2.4	15.8 ± 5.4	10.5 ± 4.6	11.9 ± 4.8	13.8 ± 8.1	12.9 ± 3.2
liver	24.2 ± 5.0	17.6 ± 4.7	16.0 ± 6.5	15.8 ± 1.4	12.8 ± 2.7	13.5 ± 7.3
spleen	11.3 ± 1.2	14.2 ± 5.3	15.0 ± 5.1	14.9 ± 5.2	12.6 ± 6.5	10.8 ± 5.3
stomach	6.7 ± 1.4	3.1 ± 0.2	2.5 ± 0.7	2.0 ± 0.5	1.9 ± 0.4	1.8 ± 0.3
small intestine	8.4 ± 1.7	6.3 ± 0.3	7.9 ± 2.9	4.8 ± 1.1	3.8 ± 0.9	4.4 ± 0.8
large intestine	4.5 ± 1.0	2.1 ± 0.6	1.7 ± 0.2	2.3 ± 0.9	1.0 ± 0.3	1.4 ± 0.5
kidney	15.9 ± 5.4	13.3 ± 1.2	7.0 ± 1.3	11.6 ± 2.6	10.2 ± 0.3	8.7 ± 2.9
muscle	2.2 ± 0.6	2.3 ± 0.2	1.6 ± 0.5	2.2 ± 0.4	2.2 ± 0.2	2.5 ± 0.2
bone	12.1 ± 0.8	13.2 ± 2.4	14.6 ± 3.8	15.2 ± 1.9	14.7 ± 3.1	15.1 ± 1.5

ratios for the lungs, liver, spleen, and kidney were 6.2 ± 2.6 (72 h), 5.6 ± 1.3 (96 h), 6.6 ± 3.2 (120 h), 9.8 ± 3.4 (72 h), respectively (see Supporting Information for complete table of complete tumor/organ ratios). As in the case of ^{64}Cu-DOTA-T/N-trastuzumab, after the earliest time points, only low levels of uptake were detected in the stomach, small intestine, large intestine, and muscle. Interestingly, distinct bone uptake is also observed, with %ID/g values ranging from 12.1 ± 0.8 at 6 h to 15.2 ± 1.9 at 72 h. This is certainly not a surprise, for residual bone uptake of ^{89}Zr has been reported on a number of occasions, and a recently publication by Abou et al. has shown that bone uptake is the *in vivo* fate of a number of species of ^{89}Zr, including [^{89}Zr]Zr-oxalate, [^{89}Zr]Zr-chloride, [^{89}Zr]Zr-citrate.[34,42,66] While a full discussion of the metabolic fate of ^{89}Zr-DFO-T/N-trastuzumab or ^{89}Zr-DFO is, of course, out of the scope of this work, it is interesting to note that the bone uptake does not increase dramatically over the course of the experiment, suggesting that the majority of ^{89}Zr deposition in the bone occurs very soon after injection.

Overall, these results are generally consistent with those previously reported for ^{89}Zr-trastuzumab bioconjugates by Munnink et al. and Holland et al.[42,43] No other data have been published on the uptake of ^{89}Zr-trastuzumab in HER2-negative MDA-MB-468 tumors; however, the uptake value obtained at 24 h in this study (13.4 ± 4.1%ID/g) is remarkably similar to the value obtained at the same time point in the blocking experiment (200 μg additional unlabeled trastuzumab) performed by Holland et al. with BT-474 cells: 13.5 ± 4.8%ID/g. While this latter experiment is not, of course, directly comparable, it does help establish a baseline for the nonspecific tumor uptake of radiolabeled antibody.

Overall, two key differences are evident upon comparing the biodistribution data obtained with ^{89}Zr-DFO-T/N-trastuzumab and ^{64}Cu-DOTA-T/N-trastuzumab. The first, increased bone uptake in the ^{89}Zr-DFO-T/N-trastuzumab experiment, is easily explained: free $^{89}Zr^{4+}$ is a bone-seeking radiometal, while free $^{64}Cu^{2+}$ has not been shown to accumulate in bone. Second, the HER2-specific tumor uptake and background signal (including initial blood levels) are higher in the ^{89}Zr-DFO-T/N-trastuzumab biodistribution than at the corresponding time points in the ^{64}Cu-DOTA-T/N-trastuzumab experiment. For example, at 6 h, the blood levels for ^{89}Zr-DFO-T/N-trastuzumab are 42.2 ± 8.8%ID/g, while they are 19.2 ± 5.2%ID/g for ^{64}Cu-DOTA-T/N-trastuzumab. Later, at 48 h, the uptake in the HER2-positive BT-474 tumor for ^{89}Zr-DFO-T/N-trastuzumab is 72.2 ± 7.9%ID/g, while for ^{64}Cu-DOTA-T/N-trastuzumab, it is 44.0 ± 7.7%ID/g. Moreover, at 48 h, the liver uptake of ^{89}Zr-DFO-T/N-trastuzumab stands at 12.8 ± 2.7%ID/g, while it is 6.4 ± 0.2%ID/g for ^{64}Cu-DOTA-T/N-trastuzumab at the same time point. It is possible that these variations in background uptake result from differences in the metabolism of the ^{89}Zr-DFO- and ^{64}Cu-DOTA-modified antibodies. The increase in HER2-specific uptake of the ^{89}Zr-DFO-T/N-trastuzumab is somewhat more puzzling, though these data are consistent with that obtained in other investigations of ^{64}Cu- and ^{89}Zr-trastuzumab.[42,65] In the case of small peptides, it has been previously reported that the identity of the radiometal may play a role in the uptake of otherwise identical radiopharmaceuticals;[67] however, given the vast size of antibodies, it is far less likely that the identity of the radiometal would exert as strong an influence in this case. Experiments are currently underway to further elucidate the origins of the differences between the pharmacodynamics of two conjugates.

Despite these differences, the biodistribution data plainly illustrate that both radiolabeled constructs are selectively and significantly taken up in the HER2-positive tumors. In addition, and perhaps more important in light of the goals of the investigation, the overall trends observed in uptake and tumor/organ ratio are strikingly similar in the two experiments.

Small Animal PET Imaging. Small animal PET imaging experiments were performed in order to further evaluate the *in vivo* behavior of the two radiometalated bioconjugates. In each case, nude mice (n = 5 for each construct) bearing bilateral BT-474 (HER2-positive) and MDA-MB-468 (HER2-negative) xenografts were injected via tail vein with either ^{64}Cu-DOTA-T/N-trastuzumab (11.1−12.9 MBq [300−345 μCi]) or ^{89}Zr-DFO-T/N-trastuzumab (10.7−11.8 MBq [290−320 μCi]). The animals were subsequently imaged periodically from injection (t = 0 h) to 48 h (^{64}Cu) or 120 h (^{89}Zr). The results clearly indicate that both constructs are taken up significantly and selectively in the HER2-positive BT-474 tumors (shown in Figures 3 and 4). In the case of ^{64}Cu-DOTA-T/N-trastuzumab, high blood pool activity and some background uptake are evident at the early time points, but over the course of the experiment, the

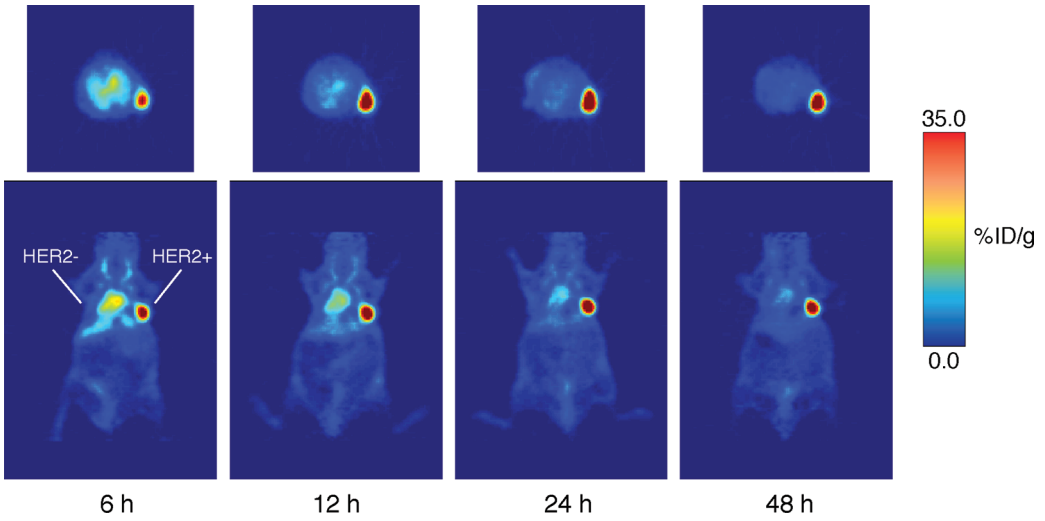

Figure 3. PET images of ^{64}Cu-DOTA-T/N-trastuzumab (11.1−12.9 MBq [300−345 μCi] in 200 μL 0.9% sterile saline) in mice bearing bilateral BT-474 (HER2-positive, right shoulder) and MDA-MB-468 (HER2-negative, left shoulder) tumors between 6 and 48 h postinjection. The transverse (top) and coronal (bottom) planar images intersect the center of the tumors.

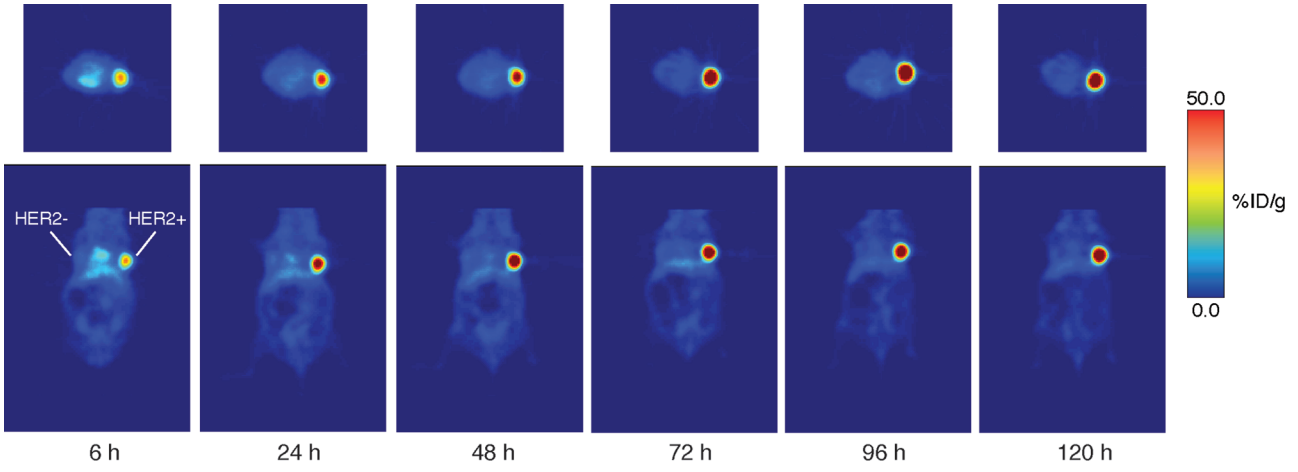

Figure 4. PET images of ^{89}Zr-DFO-T/N-trastuzumab (10.7−11.8 MBq [290−320 μCi] in 200 μL 0.9% sterile saline) in mice bearing bilateral BT-474 (HER2-positive, right shoulder) and MDA-MB-468 (HER2-negative, left shoulder) tumors between 6 and 120 h postinjection. The transverse (top) and coronal (bottom) planar images intersect the center of the tumors.

signal in the BT-474 tumor increases significantly to a point at which it is easily the most intense feature in the PET image. Similarly, for ^{89}Zr-DFO-T/N-trastuzumab, some blood pool activity is evident at the earliest time point, but the tumor uptake increases steadily in the subsequent time points along with a concomitant decrease in any background activity. The images produced by the two conjugates are very similar, a result that is consistent with the sum of the data collected in this investigation. In each case, very little background uptake is evident in either the HER2-negative MDA-MB-468 tumor or other organs. The only significant differences, as in the biodistribution experiments, are enhanced tumor and background uptake in the ^{89}Zr-DFO-T/N-trastuzumab images compared to those from ^{64}Cu-DOTA-T/N-trastuzumab and slight bone uptake of the former construct. The bone uptake is not evident in the images displayed in Figure 5 but can be spotted (though faint) in a maximum intensity projection (see Supporting Information). Just as important as the imaging similarities between the two constructs in this study, the images obtained here are consistent with those reported for other ^{89}Zr- and ^{64}Cu-trastuzumab radioagents in the literature.

Radiolabeling Trastuzumab with a Two-Step Ligation Strategy. The modular strategy described to this point comprises three simple steps: norbornene modification, tetrazine-chelator ligation, and radiometalation. However, the versatility of the tetrazine-norbornene ligation makes an alternate route possible as well: a two-step procedure in which a norbornene-modified antibody is reacted with a radiometalated, chelator-modified tetrazine (Figure 5). Indeed, similar ligations of dienophiles with radiolabeled tetrazines have already been employed with success with ^{18}F and ^{111}In, though in these cases, a transcyclooctene dienophile was employed rather than a norbornene.[29−31] To demonstrate the feasibility of such a strategy with PET radiometals, Tz-DOTA (5 nmol) was radiolabeled with ^{64}Cu (1.1−1.5 mCi) in 50 mM NH_4OAc pH 5.5 via incubation at 85 °C for 1 h (n = 3 trials). After the 1 h incubation, the labeling reaction was purified via radio-HPLC, and the product was obtained in an uncorrected

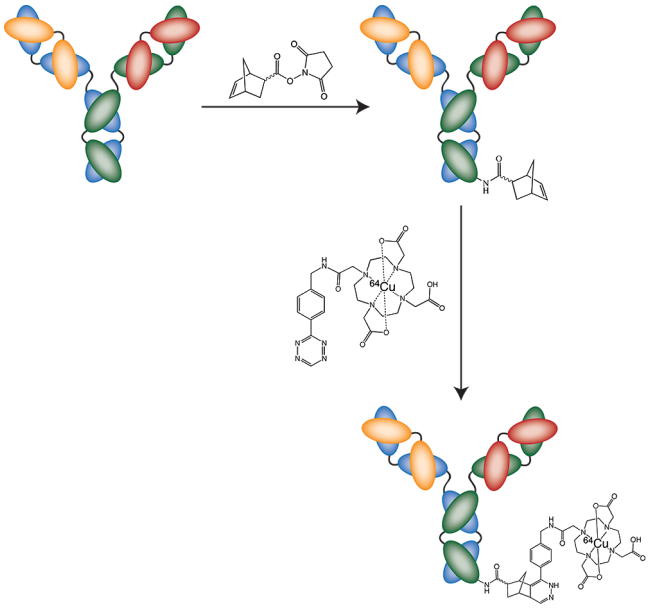

Figure 5. Schematic of the two-step radiolabeling strategy based on the ligation of norbornene-modified antibody and ^{64}Cu-labeled Tz-DOTA.

radiochemical yield of 80 ± 3% with greater than 99% radiochemical purity and a specific activity of 160 ± 5 mCi/μmol. Subsequently, this ^{64}Cu-Tz-DOTA was incubated with norbornene-modified trastuzumab (0.4 mg, 1.3 nmol, initial norbornene/mAb stoichiometry of 5:1) in PBS pH 7.4 (200 μL) at 37 °C. The progress of the reaction was monitored with radio-TLC, and after 3 h, the reaction was gauged to have reached completion. After purification via centrifugal filtration, the completed ^{64}Cu-DOTA-T/N-trastuzumab conjugate was isolated in ~75% radiochemical yield and in >99% radiochemical purity with a specific activity of 1.0 ± 0.4 mCi/mg. Granted, this specific activity is somewhat lower than that obtained with the three-step method; however, further optimization, though outside of the scope of the work at hand, could no doubt raise this specific activity to levels on par with that achieved with the three-step strategy.

Ultimately, it is our belief that the three-step method is preferable as a modular strategy for radiolabeling antibodies. This method holds the key advantage of only involving a single and relatively rapid radiochemical step, thereby minimizing the amount of radiochemistry needed for the creation of the bioconjugates while simultaneously maximizing specific activities. However, it is clear from the work currently in the literature —particularly that of Devaraj et al. and Rossin et al.—that the two-step method holds significant potential as a strategy for pretargeted antibody or peptide imaging.[23,24,27−29,31] In this application, a dienophile-modified biomolecule is first injected into a tumor-bearing animal and is permitted time to achieve its optimal biodistribution. Subsequently, a fluorophore- or radionuclide-modified tetrazine moiety is injected into the same animal and, due to the bioorthogonal nature of the tetrazine-dienophile ligation, could selectively react with the dienophile-modified biomolecule, resulting in specific localization of the marker. Indeed, both the optical and nuclear pretargeting strategies have shown very promising results. It is important to note, though, that the pretargeting systems described in the literature employ more reactive, less stable trans-cyclooctene dienophiles instead of the more stable, less reactive norbornene dienophile used in this study. Experiments are currently underway toward the creation of a pretargeting system for positron-emitting radiometals employing more reactive dienophiles.

CONCLUSION

In summary, herein we report the development of a modular system for the radiometalation of antibodies using the inverse electron demand Diels−Alder cycloaddition between tetrazine and norbornene. The strategy involves three facile, rapid, and biocompatible steps: modification of an antibody with norbornene, ligation of a chelator-modified tetrazine, and radiometalation. In this proof of concept investigation, the methodology was employed to create bioconjugates of the HER2-specific antibody trastuzumab bearing the positron-emitting radiometals ^{64}Cu and ^{89}Zr in high radiochemical purity and specific activity. For a given initial loading of norbornene, the DOTA- and DFO-modified constructs were shown to have identical numbers of chelates per antibody, and all of the radiolabeled ^{64}Cu-DOTA- and ^{89}Zr-DFO-bioconjugates displayed high serum stability and immunoreactivity. Finally, both radiolabeled bioconjugates were used in *in vivo* biodistribution and PET imaging studies with mice bearing HER2-positive (BT-474) and HER2-negative (MDA-MB-468) breast cancer xenografts. Both antibody constructs were shown to have significant and specific uptake in the HER2-positive tumor with low uptake in the HER2-negative tumor and other tissues.

This strategy does not necessarily offer a significant improvement in facility compared to popular DOTA-NHS or DFO-NCS antibody modification protocols; more importantly, however, it creates a modular platform in which a common, covalently modified antibody can be modified with a wide variety of chelators and radiometals. Given that different radiometals often require different chelators—and thus the use and optimization of different modification pathways—this methodology could no doubt aid in the rapid and robust construction of diverse radiopharmaceuticals from a single antibody stock. Further, this modular system could facilitate the creation of meaningful comparisons between bioconjugates labeled with different radiometals: as we have shown, because the chelator-modified antibodies are synthesized using identical ligation conditions, the immunoreactivity and chelator/antibody ratios of the resultant bioconjugates are likewise nearly identical regardless of the identity of the tetrazine−chelator pair.

Ultimately, therefore, this modular methodology has the potential not only to significantly aid in the synthesis and development of new radiometalated bioconjugates for PET, SPECT, and radiotherapy, but also to advance cross-pollination and constructive comparisons between radiopharmaceuticals employing diverse metallic radionuclides.

ASSOCIATED CONTENT

Supporting Information. Tables of tumor to muscle uptake ratios from ^{89}Zr-DFO-T/N-trastuzumab and ^{64}Cu-DOTA-T/N-trastuzumab biodistribution experiments and maximum intensity projection PET image of ^{89}Zr-DFO-T/N-trastuzumab indicating residual bone uptake. This material is available free of charge via the Internet at http://pubs.acs.org.

AUTHOR INFORMATION

Corresponding Author

*Phone: 1-646-888-3039. Fax: 1-646-888-3059. E-mail: lewisj2@mskcc.org.

ACKNOWLEDGMENT

The authors thank Dr. Jason P. Holland for insight and helpful conversations, Valerie Longo for aid with animal imaging experiments, Nicholas Ramos for aid in the purification of ^{89}Zr, and Alexander Veach for technical assistance. Services provided by the MSKCC Small-Animal Imaging Core Facility were supported in part by NIH grants R24 CA83084 and P30 CA08748. The authors also thank the NIH (Award 1F32CA1440138-01, BMZ; Award R01EB010011, RW) and the DOE (Award DE-SC0002184, JSL) for their generous funding.

REFERENCES

(1) van Dongen, G. A. M. S., Visser, G. W. M., Lub-de Hooge, M. N., de Vries, E. G., and Perk, L. R. (2007) Immuno-PET: a navigator in monoclonal antibody development and applications. *Oncologist 12*, 1379–1389.

(2) Wu, A. M. (2009) Antibodies and antimatter: The resurgence of immuno-PET. *J. Nucl. Med. 50*, 2–5.

(3) Zalutsky, M. R., and Lewis, J. S. (2003) Radiolabeled antibodies for tumor imaging and therapy. *Handb. Radiopharm.* 685–714.

(4) Verel, I., Visser, G. W. M., Vosjan, M. J. W. D., Finn, R., Boellaard, R., and Van Dongen, G. A. M. S. (2004) High-quality 124I-labelled monoclonal antibodies for use as PET scouting agents prior to 131I-radioimmunotherapy. *Eur. J. Nucl. Med. Mol. Imaging 31*, 1645–1652.

(5) Anderson, C. J., and Welch, M. J. (1999) Radiometal-labeled agents (non-technetium) for diagnostic imaging. *Chem. Rev. 99*, 2219–2234.

(6) Wadas, T. J., Wong, E. H., Weisman, G. R., and Anderson, C. J. (2010) Coordinating radiometals of copper, gallium, indium, yttrium, and zirconium for PET and SPECT imaging of disease. *Chem. Rev. 110*, 2858–2902.

(7) Nayak, T. K., and Brechbiel, M. W. (2009) Radioimmunoimaging with longer-lived positron-emitting radionuclides: potentials and challenges. *Bioconjugate Chem. 20*, 825–841.

(8) Divgi, C. R., Pandit-Taskar, N., Jungbluth, A. A., Reuter, V. E., Gönen, M., Ruan, S., Pierre, C., Nagel, A., Pryma, D. A., Humm, J., Larson, S. M., Old, L. J., and Russo, P. (2007) Preoperative characterisation of clear-cell renal carcinoma using iodine-124-labelled antibody chimeric G250 (124I-cG250) and PET in patients with renal masses: a phase I trial. *Lancet Oncol. 8*, 304–310.

(9) Wadas, T. J., Wong, E. H., Weisman, G. R., and Anderson, C. J. (2007) Copper chelation chemistry and its role in copper radiopharmaceuticals. *Curr. Pharm. Des. 13*, 3–16.

(10) Zeglis, B., and Lewis, J. S. (2011) A practical guide to the construction of radiometallation bioconjugates for positron emission tomography. *Dalton Trans.*

(11) Kolb, H. C., Finn, M. G., and Sharpless, K. B. (2001) Click chemistry: diverse chemical function from a few good reactions. *Angew. Chem., Int. Ed. 40*, 2004–2021.

(12) Lim, R. K. V., and Lin, Q. (2010) Bioorthogonal chemistry: recent progress and future directions. *Chem. Commun. 46*, 1589–1600.

(13) Sletten, E. M., and Bertozzi, C. R. (2009) Bioorthogonal chemistry: fishing for selectivity in a sea of functionality. *Angew. Chem., Int. Ed. 48*, 6973–6998.

(14) Moses, J. E., and Moorhouse, A. D. (2007) The growing applications of click chemistry. *Chem. Soc. Rev. 36*, 1249–1262.

(15) Glaser, M., and Robins, E. G. (2009) 'Click labelling' in PET radiochemistry. *J. Labelled Compd. Radiopharm. 52*, 407–414.

(16) Mindt, T. L., Muller, C., Stuker, F., Salazar, J. F., Hohn, A., Mueggler, T., Rudin, M., and Schibli, R. (2009) A "click chemistry" approach to the efficient synthesis of multiple imaging probes derived from a single precursor. *Bioconjugate Chem. 20*, 1940–1949.

(17) Nwe, K., and Brechbiel, M. W. (2009) Growing applications of "click chemistry" for bioconjugation in contemporary biomedical research. *Cancer Biother. Radiopharm. 24*, 289–301.

(18) Wang, C., Wang, N., Zhou, W., Shen, Y. M., and Zhang, L. (2010) Application of "click chemistry" in synthesis of radiopharmaceuticals. *Progress Chem. 22*, 1591–1602.

(19) Schultz, M. K., Parameswarappa, S. G., and Pigge, F. C. (2010) Synthesis of a DOTA-biotin conjugate for radionuclide chelation via Cu-free click chemistry. *Org. Lett. 12*, 2398–2401.

(20) Martin, M. E., Parameswarappa, S. G., O'Dorisio, M. S., Pigge, F. C., and Schultz, M. K. (2010) A DOTA-peptide conjugate by copper-free click chemistry. *Bioorg. Med. Chem. Lett. 20*, 4805–4807.

(21) Lebedev, A. Y., Holland, J. P., and Lewis, J. S. (2009) Clickable bifunctional radiometal chelates for peptide labeling. *Chem. Commun. 46*, 1706–1708.

(22) Knor, S., Modlinger, A., Poethko, T., Schottelius, M., Wester, H. J., and Kessler, H. (2007) Synthesis of novel 1,4,7,10-tetraazacyclodecane-1,4,7,10-tetraacetic acid (DOTA) derivatives for chemoselective attachment to unprotected polyfunctionalized compounds. *Chem.—Eur. J. 13*, 6082–6090.

(23) Devaraj, N. K., Upadhyay, R., Hatin, J. B., Hilderbrand, S. A., and Weissleder, R. (2009) Fast and sensitive pretargeted labeling of cancer cells through a tetrazine/trans-cyclooctene cycloaddition. *Angew. Chem., Int. Ed. 48*, 7013–7016.

(24) Devaraj, N. K., Weissleder, R., and Hilderbrand, S. A. (2008) Tetrazine-based cycloadditions: application to pretargeted live cell imaging. *Bioconjugate Chem. 19*, 2297–2299.

(25) Blackman, M. L., Royzen, M., and Fox, J. M. (2008) Tetrazine ligation: fast bioconjugation based on inverse electron demand Diels-Alder reactivity. *J. Am. Chem. Soc. 130*, 13518–13519.

(26) Schoch, J., Wiessler, M., and Jaschke, A. (2010) Post-synthetic modification of DNA by inverse-electron-demand Diels−Alder reaction. *J. Am. Chem. Soc. 132*, 8846–8847.

(27) Devaraj, N. K., Hilderbrand, S., Upadhyay, R., Mazitschek, R., and Weissleder, R. (2010) Bioorthogonal turn-on probes for imaging small molecules inside living cells. *Angew. Chem., Int. Ed. 49*.

(28) Haun, J. B., Devaraj, N. K., Hilderbrand, S., Lee, H., and Weissleder, R. (2010) Bioorthogonal chemistry amplifies nanoparticle binding and enhances the sensitivity of cell detection. *Nat. Nanotechnol. 5*, 660–665.

(29) Rossin, R., Verkerk, P. R., van den Bosch, S. M., Vulders, R. C. M., Verel, I., Lub, J., and Robillard, M. S. (2010) In vivo chemisry for pretargeted tumor imaging in live mice. *Angew. Chem., Int. Ed. 49*, 3375–3378.

(30) Li, Z., Cai, H., Hassink, M., Blackman, M., Brown, R. C. D., Conti, P. S., and Fox, J. M. (2010) Tetrazine-trans-cyclooctene ligation for the rapid construction of 18-F labeled probes. *Chem. Commun. 46*, 8043–8045.

(31) Reiner, T., Keliher, E. J., Earley, S., Marinelli, B., and Weissleder, R. (2011) Synthesis and in vivo imaging of a 18F-labeled PARP1 inhibitor using a chemically orthogonal scavenger-assisted high-performance method. *Angew. Chem., Int. Ed. 50*, 1922–1925.

(32) Meijs, W. E., Haisma, H. J., Klok, R. P., vanGog, F. B., Kievit, E., Pinedo, H. M., and Herscheid, J. D. M. (1997) Zirconium-labeled monoclonal antibodies and their distribution in tumor-bearing nude mice. *J. Nucl. Med. 38*, 112–118.

(33) Meijs, W. E., Herscheid, J. D. M., Haisma, H. J., and Pinedo, H. M. (1992) Evaluation of desferal as a bifunctional chelating agent for labeling antibodies with Zr-89. *Appl. Radiat. Isotop. 43*, 1443–1447.

(34) Holland, J. P., Divilov, V., Bander, N. H., Smith-Jones, P. M., Larson, S. M., and Lewis, J. S. (2010) Zr-89-DFO-J591 for immunoPET of prostate-specific membrane antigen expression in vivo. *J. Nucl. Med. 51*, 1293–1300.

(35) Hanahan, D., and Weinberg, R. A. (2000) The hallmarks of cancer. *Cell 100*, 57–70.

(36) Baselga, J., and Swain, S. M. (2009) Novel anticancer targets: revisiting ERBB2 and discovering ERBB3. *Nat. Rev. Cancer 9*, 463–475.

(37) Ellis, C. M., Dyson, M. J., Stephenson, T. J., and Maltby, E. L. (2005) HER2 amplification status in breast cancer: a comparison between immunohistochemical stainging and fluorescence in situ hybridisation using manual and automated quantitative image analysis scoring techniques. *J. Clin. Pathol. 58*, 710–714.

(38) Hanahan, D., Weinberg, R. A. Hallmarks of cancer: the next generation. *Cell 144*, 646-674.

(39) Slamon, D. J., Leyland-Jones, B., Shak, S., Fuchs, H., Paton, V., Bajamonde, A., Fleming, T., Eiermann, W., Wolter, J., Pegram, M., Baselga, J., and Norton, L. (2001) Use of chemotherapy plus a monoclonal antibody against HER2 for metastatic breast cancer that overexpresses HER2. *N. Engl. J. Med. 344*, 783–92.

(40) Tolmachev, V., Velikyan, I., Sandstrom, M., and Orlova, A. (2010) A HER2-binding Affibody molecule labelled with Ga-68 for PET imaging: direct in vivo comparison with the In-111-labelled analogue. *Eur. J. Nucl. Med. Mol. Imaging 37*, 1356–1367.

(41) Tang, Y., Wang, J., Scollard, D. A., Mondal, H., Holloway, C., Kahn, H. J., and Reilly, R. M. (2005) Imaging of HER2/neu-positive BT-474 human breast cancer xenografts in athymic mice using 111In-trastuzumab (Herceptin) Fab fragments. *Nucl. Med. Biol. 32*, 51–58.

(42) Holland, J. P., Caldas-Lopes, E., Divilov, V., Longo, V. A., Taldone, T., Zatorska, D., Chiosis, G., and Lewis, J. S. (2010) Measuring the pharmacodynamic effects of a novel Hsp90 inhibitor on HER2/neu expression in mice using Zr-89-DFO-trastuzumab. *PLOS One 5*.

(43) Munnink, T. H. O., de Korte, M. A., Nagengast, W. B., Timmer-Bosscha, H., Schroder, C. P., de Jong, J. R., van Dongen, G., Jensen, M. R., Quadt, C., Lub-de Hooge, M. N., and de Vries, E. G. E. (2010) Zr-89-trastuzumab PET visualises HER2 downregulation by the HSP90 inhibitor NVP-AUY922 in a human tumour xenograft. *Eur. J. Cancer 46*, 678–684.

(44) Dijkers, E. C. F., Kosterink, J. G. W., Rademaker, A. P., Perk, L. R., van Dongen, G. A. M. S., Bart, J., de Jong, J. R., de Vries, E. G. E., and Lub-de Hooge, M. N. (2009) Development and characterization of clinical-grade 89Zr-trastuzumab for HER2/neu immunolPET imaging. *J. Nucl. Med. 50*, 974–981.

(45) Niu, G., Li, Z., Cao, Q., and Chen, X. (2009) Monitoring therapeutic response of human ovarian cancer with 17-DMAG by noninvasive PET imaging with ^{64}Cu-DOTA-trastuzumab. *Eur. J. Nucl. Med. Mol. Imaging*.

(46) Smith-Jones, P. M., Solit, D. B., Afroze, F., Rosen, N., and Larson, S. M. (2006) Early tumor response to Hsp90 therapy using HER2 PET: Comparison with 18F-FDG PET. *J. Nucl. Med. 47*, 793–796.

(47) Garmestani, K., Milenic, D. E., Plascjak, P. S., and Brechbiel, M. W. (2002) A new and convenient method for purification of 86Y using a Sr(II) selective resin and comparison of biodistribution of 86Y and 111In labeled Herceptin. *Nucl. Med. Biol. 29*, 599–606.

(48) Verel, I., Visser, G. W. M., Boellaard, R., Stigter-van Walsum, M., Snow, G. B., and van Dongen, G. (2003) Zr-89 immuno-PET: Comprehensive procedures for the production of Zr-89-labeled monoclonal antibodies. *J. Nucl. Med. 44*, 1271–1281.

(49) Zanzonico, P. (2009) Routine quality control of clinical nuclear medicine instrumentation: a brief review. *J. Nucl. Med. 49*, 1114–1131.

(50) McCarthy, D. W., Shefer, R. E., Klinkowstein, R. E., Bass, L. A., Margeneau, W. H., Cutler, C. S., Anderson, C. J., and Welch, M. J. (1997) Efficient production of high specific activity Cu-64 using a biomedical cyclotron. *Nucl. Med. Biol. 24*, 35–43.

(51) Holland, J. P., Sheh, Y. C., and Lewis, J. S. (2009) Standardized methods for the production of high specific-activity zirconium-89. *Nucl. Med. Biol. 36*, 729–739.

(52) Anderson, C. J., Connett, J. M., Schwarz, S. W., Rocque, P. A., Guo, L. W., Philpott, G. W., Zinn, K. R., Meares, C. F., and Welch, M. J. (1992) Copper-64-labeled antibodies for PET imaging. *J. Nucl. Med. 33*, 1685–1691.

(53) Anderson, C. J., Schwarz, S. W., Connett, J. M., Cutler, P. D., Guo, L. W., Germain, C. J., Philpott, G. W., Zinn, K. R., Greiner, D. P., Meares, C. F., and Welch, M. J. (1995) Preparation, biodistribution, and dosimetry of copper-64-labeled anti-colorectal carcinoma monoclonal-antibody gragments 1A3-F(AB′)(2). *J. Nucl. Med. 36*, 850–858.

(54) Lindmo, T., Boven, E., Cuttitta, F., Fedorko, J., and Bunn, P. A., Jr. (1984) Determination of the immunoreactive fraction of radiolabeled monoclonal antibodies by linear extrapolation to binding at infinite antigen excess. *J. Immunol. Methods 72*, 77–89.

(55) Lindmo, T., and Bunn, P. A., Jr. (1986) Determination of the true immunoreactive fraction of monoclonal antibodies after radiolabeling. *Methods Enzymol. 121*, 678–91.

(56) Kim, J. S., Lee, J. S., Im, K. C., Kim, S. J., Kim, S.-Y., Lee, D. S., and Moon, D. H. (2007) Performance measurement of the microPET Focus 120 scanner. *J. Nucl. Med. 48*, 1527–1535.

(57) Kampchen, T., Massa, W., Overheu, W., Schmidt, R., and Seitz, G. (1982) Zur kenntnis von reaktionen des 1,2,4,5-tetrazin-3,6-dicarbonsaure-dimethylesters mit nucleophilen. *Chem. Ber. 115*, 683–694.

(58) Lin, C. H., Lieber, E., and Horwitz, J. P. (1954) The synthesis of syn-diaminotetrazine. *J. Am. Chem. Soc. 76*, 427–430.

(59) Solducho, J., Doskocz, J., Cabaj, J., and Roszak, S. (2003) Practical synthesis of bis-substituted tetrazine with two pendant 2-pyrrolyl or 2-thienyl groups, precursors of new conjugated polymers. *Tetrahedron 59*, 4761–4766.

(60) Vosjan, M., Perk, L. R., Visser, G. W. M., Budde, M., Jurek, P., Kiefer, G. E., and van Dongen, G. (2010) Conjugation and radiolabeling of monoclonal antibodies with zirconium-89 for PET imaging using the bifunctional chelate p-isothiocyanatobenzyl-desferrioxamine. *Nat. Protoc. 5*, 739–743.

(61) Verel, I., Visser, G. W. M., Boellaard, R., Stigter-van Walsum, M., Snow, G. B., and van Dongen, G. A. M. S. (2003) ^{89}Zr immuno-PET: comprehensive procedures for the production of ^{89}Zr-labeled monoclonal antibodies. *J. Nucl. Med. 44*, 1271–1281.

(62) Brouwers, A., Verel, I., Van Eerd, J., Visser, G., Steffens, M., Oosterwijk, E., Corstens, F., Oyen, W., Van Dongen, G., and Boerman, O. (2004) PET radioimmunoscintigraphy of renal cell cancer using Zr-89-labeled cG250 monoclonal antibody in nude rats. *Cancer Biother. Radiopharm. 19*, 155–163.

(63) Niu, G., Li, Z., Xie, J., Le, Q.-T., and Chen, X. (2009) PET of EGFR antibody distribution in head and neck squamous cell carcinoma models. *J. Nucl. Med. 50*, 1116–1123.

(64) Martin, S. M., O'Donnell, R. T., Kukis, D. L., Abbey, C. K., McKnight, H., Sutcliffe, J. L., and Tuscano, J. M. (2008) Imaging and pharmacokinetics of 64Cu-DOTA-HB22.7 administered by intravenous, intraperitoneal, or subcutaneous injection to mice bearing non-Hodgkin's lymphoma xenografts. *Mol. Imaging Biol. 11*, 79–87.

(65) Paudyal, P., Paudyal, B., Hanaoka, H., Oriuchi, N., Iida, Y., Yoshioka, H., Tominaga, H., Watanabe, S., Ishioka, N. S., and Endo, K. (2010) Imaging and biodistribution of Her2/neu expression in non-small cell lung cancer xenografts with 64Cu-labeled trastuzumab PET. *Cancer Sci. 101*, 1045–1050.

(66) Abou, D. S., Ku, T., and Smith-Jones, P. M. (2011) In vivo biodistribution and accumulation of 89Zr in mice. *Nucl. Med. Biol.* [Online early access].

(67) Antunes, P., Ginj, P., Zhang, H., Waser, B., Baum, R. P., Reubi, J. C., and Maecke, H. (2007) Are radiogallium-labeled DOTA-conjugated somatostatin analogues superior to those labeled with other radiometals? *Eur. J. Nucl. Med. Mol. Imaging 34*, 982–993.